

CHAPTER 14 DATA ANALYSIS SOFTWARE FOR ION BEAM ANALYSIS

Handbook of Modern Ion Beam Analysis, 2nd Edition, eds. Yongqiang Wang and Michael Nastasi, Materials Research Society, Warrendale 2010 (2009), pp 305-345.

N. P. Barradas

Instituto Tecnológico e Nuclear, Sacavém, Portugal
Centro de Física Nuclear da Universidade de Lisboa, Lisboa, Portugal

E. Rauhala

University of Helsinki, Helsinki, Finland

CONTENTS

14.1 INTRODUCTION	
14.1.1 Data analysis software.....	
14.1.2 Scope of the chapter	
14.1.3 Historical development and reviews of software programs.....	
14.2 TYPES OF CODES	
14.2.1 The direct calculation method	
14.2.2 Simulation by successive iterations.....	
14.2.3 Interactive versus automated	
14.2.4 Deterministic versus stochastic (Monte Carlo)	
14.3 CAPABILITIES OF CODES	
14.3.1 Design basis	
14.3.1.1. Techniques implemented	
14.3.1.2. Experimental conditions supported.....	
14.3.1.3. Description of samples	
14.3.2 Databases implemented.....	
14.3.2.1. Stopping power.....	
14.3.2.2. Scattering cross section.....	
14.3.3 Basic physics.....	
14.3.4 Advanced physics.....	
14.3.4.1. Straggling models.....	
14.3.4.2. Electron screening.....	
14.3.4.3. Plural scattering	
14.3.4.4. Multiple scattering	
14.3.4.5. Simulation of resonances	
14.3.4.6. Surface and interface roughness.....	
14.3.4.7. Channeling.....	
14.3.4.8. Pulse pileup.....	
14.3.5 Automated optimization	
14.3.5.1. Fitting.....	

14.3.5.2.	Bayesian inference.....	
14.3.6	Usability and usage.....	
14.4	ACCURACY.....	
14.4.1	Numerical accuracy of codes.....	
14.4.2	Intrinsic accuracy of IBA experiments.....	
14.4.2.1.	Models and basic physical quantities.....	
14.4.2.2.	Experimental conditions.....	
14.4.2.3.	Counting statistics.....	
14.4.3	Physical effects on data analysis.....	
14.5	RUMP AND FIRST-GENERATION CODES.....	
14.6	NEW-GENERATION CODES: SIMNRA AND NDF.....	
14.6.1	Further capabilities.....	
14.6.2	SIMNRA.....	
14.6.3	NDF.....	
14.6.4	Issues.....	
14.7	MONTE CARLO SIMULATION.....	
14.8	OTHER TECHNIQUES.....	
14.8.1	PIXE.....	
14.8.2	Resonant NRA, PIGE, NRP, MEIS, channeling, microscopies, and so on	
14.9	THE IBA DATA FORMAT IDF.....	
	ACKNOWLEDGEMENTS.....	
	SOFTWARE WEB SITES.....	
	REFERENCES.....	

14.1 INTRODUCTION

14.1.1 Data analysis software

The data analysis software in ion beam methods are computer programs designed to extract information about samples from the measured ion beam spectra. The desired information includes identification of sample elements, their concentrations, areal densities, and layer thicknesses. At best, one spectrum can be converted to concentration–depth distributions of all elements in the sample. Often, however, such a full description of the sample based on a single experiment is not possible. The analyst can then perform additional experiments using different experimental parameters such as ion energies or a different measurement geometry or including information from one or more other complementary techniques.

The software can also be used for designing relevant experiments. Depending on the assumed sample structure, the appropriate ion beam technique can be chosen by doing test simulations prior to experiments. For example, the most suitable parameters for the measurements can be tested. The choice of ions, energies, geometries, and so on can be examined without performing often extensive and complicated experiments.

The third main function of the software is found in education and research. By using simulation computer programs, the researcher can readily scrutinize the characteristics of various ion beam techniques. The dependencies between stopping powers, cross sections, energies, and so on can be studied. Novel reaction cross sections and stopping powers can be implemented in the programs to investigate the agreement between simulation and experimental data. Fine details, such as double and multiple scattering, screening, pileup, and the properties of various detector systems can be analyzed with the help of data analysis programs.

It cannot be overemphasized that software is an aid to data analysis and does not replace the judgment of the analyst. Software that is not correctly used, or that is used outside its scope of application, leads to wrong data analysis. Furthermore, it should be noted that the scope of application of a given program might not be clear and will depend on the details of the experiment being analyzed: for instance, Bohr straggling is adequate for analysis of normal-incidence proton Rutherford backscattering spectrometry (RBS) with a surface barrier detector, but it is completely inadequate for heavy-ion elastic recoil detection analysis (ERDA) or for high-resolution near-surface analysis, where the straggling is asymmetric.

14.1.2 Scope of the chapter

This chapter deals mainly with the data analysis software of particle–particle ion beam analysis (IBA) techniques: Rutherford backscattering spectrometry (RBS), elastic recoil detection analysis (ERDA), and nuclear reaction analysis (NRA). In the last case, we limit ourselves to techniques utilizing one single beam energy, as opposed to resonant NRA or narrow resonance profiling (NRP) [see Amsel (1996) for a discussion on acronyms]. Short sections on particle-induced X-ray emission (PIXE) spectroscopy and other techniques such as NRP and channeling are also included.

A list of Web sites relevant for IBA software and data analysis is provided at the end of the chapter, just before the list of references. Note that this list is by no means comprehensive, and in particular, that several of the codes mentioned in this chapter have no dedicated Web site.

14.1.3 Historical development and reviews of software programs

Computer programs to analyze data from RBS, NRA, and ERDA date back to the 1960s and 1970s. These techniques developed in parallel with the beginning of the new semiconductor and other high-technology industries, where new needs for ion beams in the production, modification, and characterization of novel materials were arising. IBA techniques for quantitative depth profiling in the micron range and determination of low-concentration elemental impurities were quickly recognized and widely applied. As these analytical tools became more versatile, the samples, spectra, and data analysis problems also became more complicated. By the end of the 1990s, the collection of software had developed in various directions: codes exist that can handle very general data analysis problems and various IBA techniques; some are highly automatic, whereas others treat specified problems with great exactness.

The historical development of the software was reviewed recently by Rauhala *et al.* (2006), which presents the characteristics and status of 12 software packages as of 2006. An intercomparison of several software packages for simulations and real data-analysis applications is presented in Barradas *et al.* (2007b). Relevant developments up to 2009 are also included in this chapter.

14.2 TYPES OF CODES

14.2.1 The direct calculation method

In direct spectrum analysis, the yields from separated signals of the spectrum are transformed into concentration values by closed-form analytical calculation. Other forms of direct analysis include conversion from signal areas and heights to total amounts or concentrations. This is the opposite of spectrum simulation, where a theoretical spectrum is generated from an assumed depth profile and compared to the actual data.

This approach was introduced by Børgeesen *et al.* (1982) with the code SQUEAKIE. This approach is straightforward and effective in many cases. However, it has problems because of the implementation of straggling and the stability of results as a result of uncertainties in the stopping database and measurement noise. The direct method is still used, normally as a complement to full simulations, and often in heavy-ion ERDA (Spaeth *et al.*, 1998).

14.2.2 Simulation by successive iterations

Almost all of the presently available IBA data analysis software is based on simulation by successive iterations. The simulation modeling assumes that the underlying physics, mathematics, and nuclear and atomic data are valid and adequately describe the physical processes involved. Starting from a known sample structure, the corresponding experimental energy spectrum can be theoretically simulated from a few basic data and the known formalism of the reaction spectrometry. by comparing the experimental and theoretical spectra and iteratively modifying the assumed composition of the sample, a close similarity of the spectra is typically accomplished after a few iterations. The sample structure leading to the theoretical spectrum is then taken to correspond to the material's sample structure. Erroneous results or misinterpretations of the material's

structure can result from incorrect science, ambiguous data, or inadequate software documentation and guidance for analysts to extract the correct information.

The typical iterative simulation proceeds as follows:

1. Assume the experimental parameters and the known experimental spectrum.
2. Assume an initial sample composition.
3. Calculate a theoretical spectrum corresponding to the experimental parameters and the assumed sample composition.
4. Compare the simulated spectrum to the experimental spectrum.
5. Identify the differences and modify the assumed sample composition accordingly.
6. Repeat iteration steps 3–5 until an adequate fit between the simulated and experimental spectra is accomplished.
7. Take the sample parameters corresponding to the best simulation to be the sample structure resulting from the data analysis.

This procedure is illustrated in EXAMPLE 14.1.

EXAMPLE 14.1. Convergence of iteration.

Assume that the experimental parameters and the elements in the sample are known. Start by making a guess about the sample composition. How do the iterations converge?

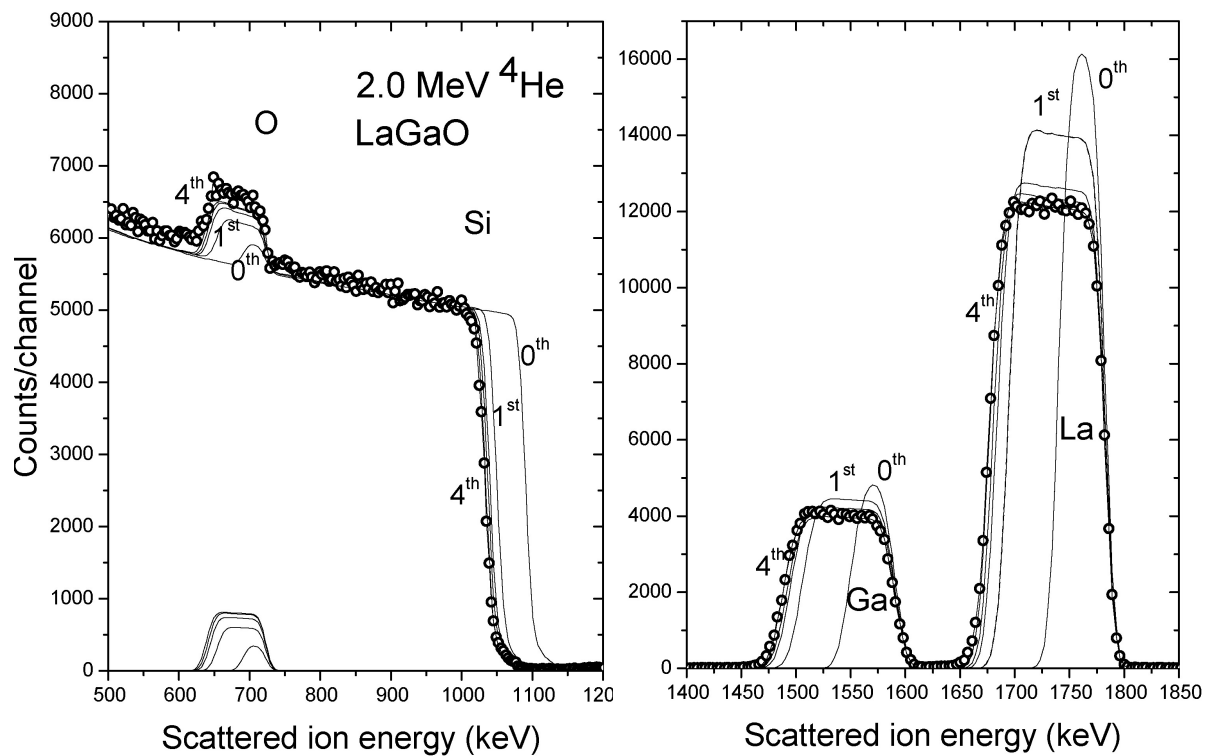


Fig. 14.1. Backscattering spectrum (\circ) for 2.00 MeV ^4He ions incident on a LaGaO layer on a silicon substrate

Figure 14.1 shows the spectrum for 2.00 MeV ^4He ions incident on a LaGaO layer on a silicon substrate. In the experiment, the following parameters were used:

Incident ^4He -ion energy, $E_{\text{He}} = 2.00 \text{ MeV}$
Scattering angle, $\theta = 170^\circ$
Angle of incidence, $\theta_1 = 50^\circ$
Solid angle \times accumulated charge, $Q\Omega = 69.0 \text{ msr } \mu\text{C}$
Energy per channel, $\delta E = 3.475 \text{ keV/channel}$
Energy in zero channel, $= 27.3 \text{ keV}$

Zeroth iteration: Initially, as a guess of the LaGaO film composition, equal concentrations of the elements in a layer of $200 \times 10^{15} \text{ at./cm}^2$ areal density were assumed.

Initial assumptions:

Equal amounts of the three elements, 33% La, 33% Ga, 33% O.
Layer areal density, $200 \times 10^{15} \text{ at./cm}^2$.

\Rightarrow 0th iteration.

The resulting simulated spectrum is denoted as the 0th iteration in Fig. 14.1. The simulated signal heights of La and Ga and the signal width of La were then compared to those of the experimental spectrum. Concentrations and layer areal density were changed assuming the same linear dependence between the signal heights and concentrations and between the signal widths and areal density of the layer.

The La concentration was thus multiplied by the ratio of the experimental La signal height to the simulated La signal height. Similarly, the areal density of the film was multiplied by the ratio of the experimental La signal width to the simulated La signal width.

This process was then repeated. The solid lines denoted as 1st, ..., 4th, in Fig. 14.1, show the results of subsequent iterations. In detail, the iteration converged as follows:

First iteration. The height of the experimental La signal was observed to be roughly 75% of the height of the simulated signal. The same ratio for Ga was observed to be 80%.

The experimental La signal was observed to be roughly 2.4 times wider than the simulated signal.

Reduce the La concentration to $75\% \times 0.33 = 0.25$.

Reduce the Ga concentration to $80\% \times 0.33 = 0.26$.

Increase the areal density of the layer to $2.4 \times 200 \times 10^{15} \text{ at./cm}^2 = 480 \times 10^{15} \text{ at./cm}^2$.

\Rightarrow 1st iteration.

Second iteration. The height of the experimental La signal was observed to be 85% of the height of the simulated signal. The same ratio for Ga was observed to be 88%.

The experimental signal was observed to be 1.2 times wider than the simulated signal.

Reduce the La concentration to $85\% \times 0.25 = 0.21$.

Reduce the Ga concentration to $88\% \times 0.26 = 0.23$.

Increase the areal density of the layer to $1.2 \times 480 \times 10^{15} \text{ at./cm}^2 = 580 \times 10^{15} \text{ at./cm}^2$.
⇒ 2nd iteration.

Third iteration. The height of the experimental La signal was observed to be 95% of the height of the simulated signal. The same ratio for Ga was observed to be 93%. The experimental signal was observed to be 1.06 times wider than the simulated signal.

Reduce the La concentration to $95\% \times 0.21 = 0.20$.
Reduce the Ga concentration to $93\% \times 0.23 = 0.21$.
Increase the areal density of the layer to $1.06 \times 580 \times 10^{15} \text{ at./cm}^2 = 615 \times 10^{15} \text{ at./cm}^2$.
⇒ 3rd iteration.

Fourth iteration. The height of the experimental La signal was observed to be 97% of the height of the simulated signal. The fit of the Ga signal was acceptable. The experimental signal was observed to be 1.04 times wider than the simulated signal.

Reduce the La concentration to $97\% \times 0.20 = 0.195$.
Maintain the Ga concentration at 0.21.
Increase the areal density of the layer to $1.04 \times 615 \times 10^{15} \text{ at./cm}^2 = 640 \times 10^{15} \text{ at./cm}^2$.
⇒ 4th iteration.

As a result of the fourth iteration, both the signal heights and the signal widths of La and Ga seem to be fitted adequately within the plotting accuracy of the figure. In practical terms, users tend to adjust the concentration and thickness values manually, without doing the exact procedure shown here. This leads to a larger number of iterations, which most users find acceptable given that the calculations are very fast with modern computers.

The crucial point in the iterative procedure is to describe the sample composition. Several codes let the user introduce functions that describe the depth profile of a given element. However, the most popular method to describe a sample is to divide it into sublayers. Each sublayer has a different composition, which is iteratively changed. Also, the number of sublayers is increased or decreased during the iterative procedure: If the current number of layers is not sufficient to reproduce the changing signals observed, the user introduces a new layer. If, on the other hand, the user can obtain an equivalent fit by using fewer layers, this is normally preferred. In practice, the depth resolution of the experiment limits the number of layers needed. This is illustrated in EXAMPLE 14.2.

EXAMPLE 14.2. Simulating composition changes by division into sublayers.

Changes of concentrations of components within a layer can be treated by dividing the layer into sublayers of constant composition. Figure 14.2 shows a spectrum for 2.75 MeV ^7Li ions incident on a PbZrSnO thin-film sample on a Si substrate (Harjuoja *et al.*, 2007). When trying to simulate the spectrum, one finds that the interface between the

film and the substrate is not well defined and that the concentrations change with depth within the thin film.

This spectrum has been simulated by assuming nine sublayers of constant composition. The simulated spectrum as a result of data analysis by the program GISA is illustrated as the thick solid line connecting the experimental data points. The theoretical signals of the elemental components in each of the sublayers are shown as thin solid lines. The thick solid line thus represents the sum of the thin lines of the elemental signals in the sublayers.

The experimental parameters, the concentrations of the elements, and the areal densities of the sublayers are given in Table 14.1. The concentrations of the elements versus areal density are shown in Fig. 14.3.

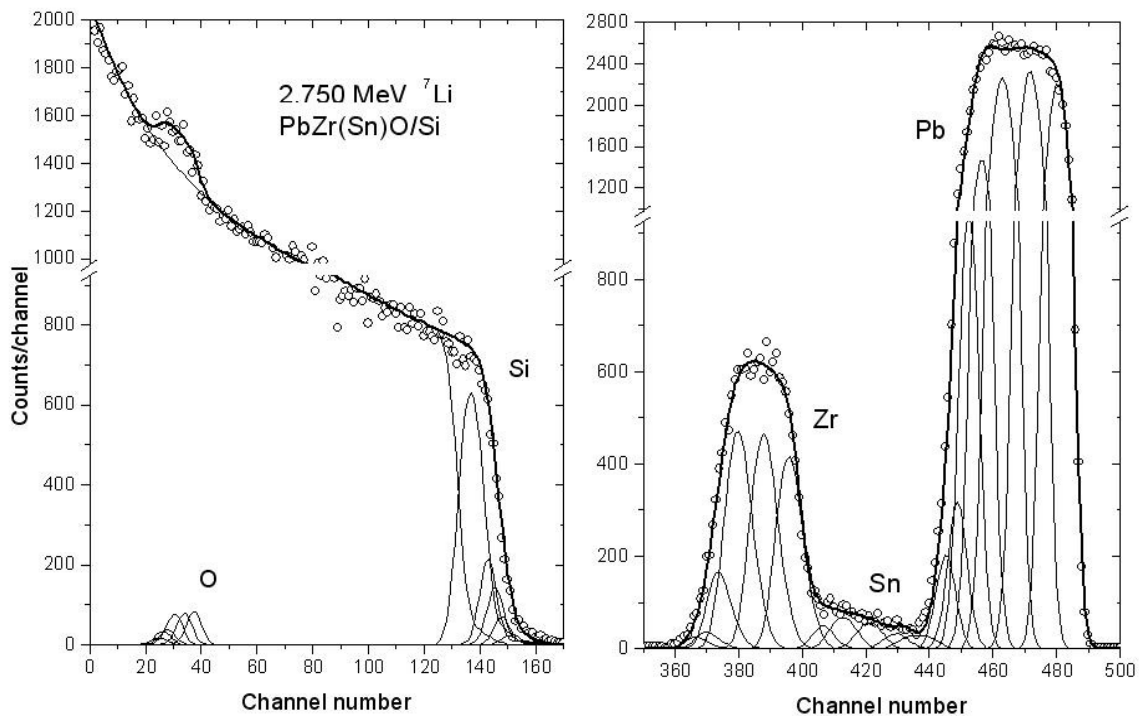
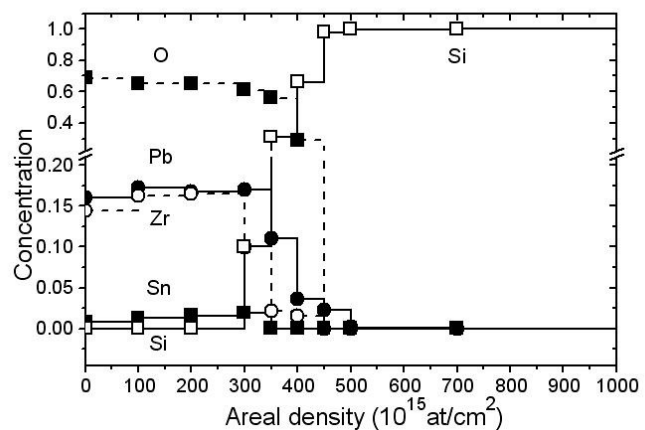


FIG. 14.2. Backscattering spectrum for 2.75 MeV ${}^7\text{Li}$ ions incident on a PbZrSnO thin-film sample on a Si substrate. The thick solid line connecting the experimental data points is the simulated spectrum.

FIG. 14.3. The constant concentrations of the elements (see Table 14.1) versus areal density. Table 14.1. Experimental parameters and concentrations of the elements and areal densities of the sublayers.



Incident particle ${}^7\text{Li}$, $E_0 = 2750$ keV, $\delta E = 4.424$ keV/channel, $Q\Omega = 9.687$ $\mu\text{C msr}$, scattering angle 165° , angle of incidence 60° , exit angle 45° , system resolution 25 keV full width at half-maximum (fwhm).

Sublayer	10^{15} at./ cm^2	Pb	Sn	Zr	Si	O
1	100	0.16	0.0075	0.145	0	0.6875
2	100	0.173	0.0128	0.163	0	0.6512
3	100	0.168	0.0155	0.165	0	0.6515
4	50	0.17	0.019	0.1	0.1	0.611
5	50	0.11	0	0.022	0.31	0.558
6	50	0.036	0	0.0153	0.66	0.2887
7	50	0.023	0	0	0.977	0
8	200	0.0015	0	0	0.9985	0
9	5000	0	0	0	1	0

None of the layers was assumed to contain any undetected light elements. The oxygen signal was not fitted; the oxygen concentration follows from the concentrations of the heavier elements, as it is presumed to make up the total fractional concentration of each sublayer to 1. Bohr straggling and a scaled stopping of 1.08 times the TRIM-91 stopping value were assumed for the metal oxide layers.

The example is intended to demonstrate how the composition variations can be treated as constant composition sublayers. As discussed in Section 14.3.4.6, the interdiffusion and interfacial roughness can usually not be distinguished by using a backscattering spectrometry. In the present case, the probable cause for the mixing of the elements at the interface is diffusion, as the atomic-layer deposition of the metal oxide film should not change the smooth Si surface.

14.2.3 Interactive versus automated

The iterative procedure can be executed in an interactive way, where the user repeatedly refines the depth profile until it is considered that better agreement cannot be reached within the time and patience limits of the user; or with an automated process based on optimization of some target function such as a χ^2 or likelihood function.

Caution is needed when using automated optimization. Different depth profiles can lead to the same simulated spectrum (Butler, 1990), and the code has no way of knowing which of the possible solutions is the correct one. The user must often restrict the solution space, for instance, by performing only a local optimization on a limited number of parameters, one at a time.

A second problem is that the χ^2 function is very sensitive to the quality of the simulation: for instance, if straggling is not included, an automated procedure will return interfacial mixing layers that might not exist. This can be solved naturally by including straggling, but there are some physical effects for which no accurate analytical simulations have been developed so far. In such cases, fully automated

processes will lead to artifacts in the depth profiles derived, unless the user restricts the solution space to physical solutions.

In any case, some form of automation is desirable, particularly if large quantities of data are to be analyzed.

14.2.4 Deterministic versus stochastic (Monte Carlo)

Deterministic codes follow a calculational procedure that is defined *a priori*. In simulations, the sample is divided into thin sublayers. Both the incoming beam energy and the detected energy for scattering on each element present are calculated for each sublayer. The simulation is then constructed based on these quantities and on the concentration of each element in each sublayer. Straggling and other physical phenomena can be included. However, individual collisions between the analyzing ion (and its electrons) and the target nuclei and electrons are not modeled.

These deterministic simulations are normally very fast, lending themselves very well to the interactive and automated procedures described above, and they are, in fact, the standard approach.

Monte Carlo codes work in a completely different, more fundamental, way. They model individual interactions between particles. In this way, phenomena that have traditionally been difficult to include in the standard method are included in a natural way. The quality of the simulations that can be reached is, in principle, much superior.

However, there are issues with the calculation times required. Even with modern computers, acceleration techniques to speed up the calculations must be used. These include, for instance, disregarding collisions with scattering angles smaller or larger than values defined *a priori* and artificially increasing the scattering cross section or the solid angle of the detector in order to have more events. In some cases, such techniques can affect the quality of the simulations.

A second issue is related to the fact that Monte Carlo codes often require very detailed knowledge about the physics involved, and so far, their use has remained mostly confined to the code authors. Until recently, almost all data analysis was performed using deterministic codes (the largest exception was the use of Monte Carlo codes for the analysis of channeling data).

Nevertheless, improvements of the calculation times, coupled with the development of user-friendly interfaces, mean that Monte Carlo codes are becoming more widespread and might become dominant in areas such as heavy-ion ERDA, where multiple scattering and special detection systems play a large role.

14.3 CAPABILITIES OF CODES

In this section, we discuss some of the considerations that are important when selecting an IBA code. We note that there is no such thing as a “best code” for all situations. All codes discussed here do well at what they were designed to do, as shown by an intercomparison exercise organized by the International Atomic Energy Agency (IAEA) (Barradas *et al.*, 2007b). No code is complete in the sense that it can analyze all possible IBA data.

The codes that took part in the IAEA intercomparison exercise were compared numerically and validated. Some of their most important characteristics are shown in Tables 14.2–14.8. Characteristics of several other codes are described in Rauhala *et al.*

(2006). We stress that all information given was valid at the time of writing, as several codes are being actively developed.

When choosing which code to use, users must consider whether a given code is capable of extracting the information required and how easy it is to do so with each code. A complex sample where interface roughness and multiple scattering play a crucial role might need a last-generation code, but to determine the thickness of a thin film with one single heavy element on a light substrate, a full Monte Carlo calculation is probably too much work without extra benefit. Also, in some cases, manual calculations with careful consideration of error sources might be the most accurate method (see, for instance, Boudreault *et al.*, 2002).

14.3.1 Design basis

The first consideration is obviously whether the data to be analyzed are within the design basis of the code considered. The two main points are the techniques implemented by each code and, for each technique, the experimental conditions supported.

For instance, if a code can only analyze RBS data with H and He beams, there is no point in trying to use it to analyze NRA data, but it might be possible to adapt it to analyze RBS with heavier ions, particularly if the source code is available.

In a similar way, even if a code includes RBS, for example, it might be limited to given experimental conditions. One example is the detection geometry: some codes include not only the well-known IBM and Cornell geometries, but also general geometry where any location of the detector is allowed (including transmission). Another consideration is the detection system, with most codes including only energy-dispersive systems, whereas some can include velocity and time-of-flight spectra, magnetic spectrometers, and others.

14.3.1.1 Techniques implemented

As stated in Section 14.1.2, this chapter is aimed predominantly at RBS and ERDA software packages. Elastic backscattering spectrometry (EBS) is, in practice, RBS with non-Rutherford cross sections that must be provided by the user (or included in the code) for each given ion/target nucleus pair.

Nonresonant NRA is also included here because it also uses one single beam energy (as opposed to resonant NRA, where the energy is scanned), and it is common that both the scattered beam and some reaction product are detected simultaneously.

Techniques such as channeling, PIXE, and resonant NRA are included in some of the codes.

Table 14.6 lists the techniques implemented in each code. All implement RBS, but some do not include ERDA or NRA. The code NDF is the only one to include PIXE. Note, however, that some laboratories perform only RBS, and it might be convenient to use a code with fewer options (and thus possibly easier to use) that can do what the user needs and nothing else. However, most laboratories employ several techniques, and using the same code to analyze all of the data has obvious advantages.

14.3.1.2 Experimental conditions supported

Table 14.6 also includes the experimental conditions supported by each code. They are similar for all codes, which handle most situations. Some differences exist, however, and users who need special conditions should consider carefully the varying capabilities of the codes. Also, it might be possible to convince authors of codes still under development to implement some specific experimental conditions not previously covered. If the source code is available, expert users can modify the supported experimental conditions according to their convenience.

14.3.1.3 Description of samples

One of the most important points in codes is how conveniently the sample can be described. This is illustrated in Table 14.8.

Homogeneous layers are considered in all codes that participated in the IAEA intercomparison exercise and in almost all codes known to us. In some codes, functions describing continuous profiles can also be introduced, which is important if, for instance, diffusion of implant profiles are being analyzed.

Sometimes, a maximum number of layers or of elements within a given layer is imposed. When restrictions on the number of layers exist, problems can arise when a very thin layer description is required. This is the case for samples with many thin layers and for high-resolution experiments (for instance, using a magnetic spectrometer or grazing-angle geometry).

RBS spectra are ambiguous whenever more elements are present than spectra were collected (Butler, 1990; Alkemade *et al.*, 1990). In that case, more than one different depth profile can lead to exactly the same simulated spectrum. To remove ambiguities, more spectra should be collected, with different experimental conditions. However, often, the elements are bound in molecules, allowing the analyst to relate the respective signals to each other; for instance, if SiO₂ is present, the small O signal can be related to the much larger Si signal by imposing the known stoichiometry. One very useful function in a code is therefore to allow the user to use as logical fitting elements not only atomic species, but molecules as well. The molecules can be of known or unknown composition. In the latter case, such a code would fit the molecular stoichiometry together with its concentration in each layer. One example of such an approach is discussed in Chapter 15, Pitfalls in Ion Beam Analysis.

In Fig. 14.4, we show the RBS spectra of a 21-layer ZrO₂/SiO₂ antireflection coating with a top Au layer (Jeynes *et al.*, 2000a). The Zr had a small (known) amount of Hf contamination. Both normal incidence and a 45° angle of incidence were used. The O, Si, and Hf signals are small and superimposed on the much larger Zr signal. It is virtually impossible to analyze these data meaningfully without introducing the chemical information in some way. Consequently, the two spectra were fitted simultaneously, with the known molecules imposed as logical fitting elements. The small ~5% misfits might be due to inaccurate stopping or small deviations from stoichiometry. In any case, complete disambiguation of the data is achieved.

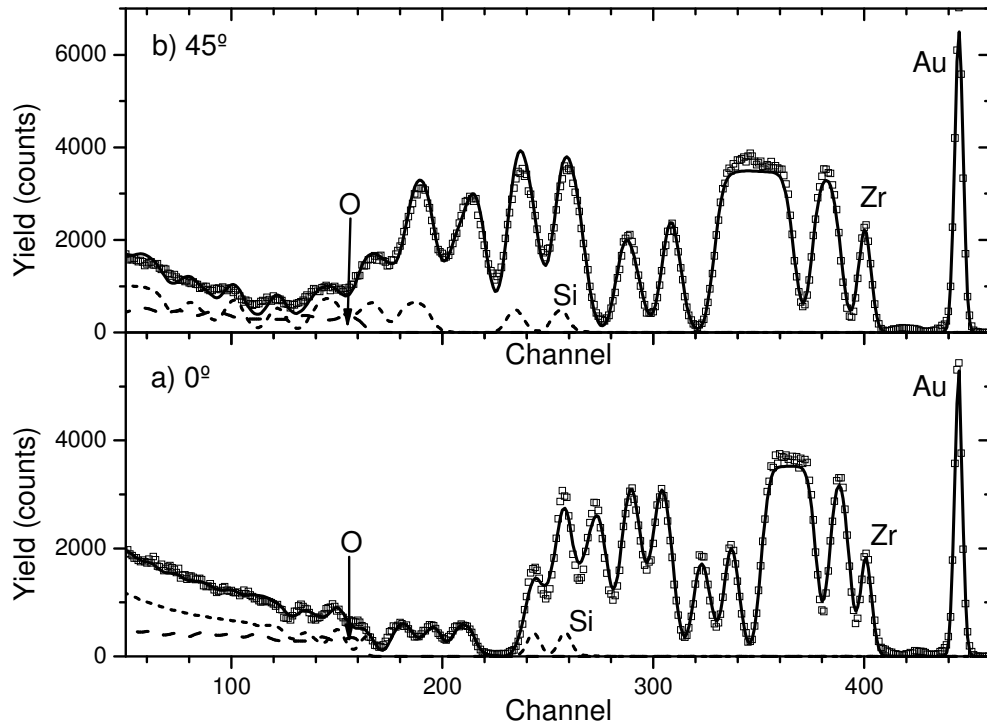


FIG 14.4. Data and fit (solid line) obtained for a 21-layer ZrO_2/SiO_2 antireflection coating with a top Au layer, shown for the data collected at (a) normal and (b) 45° incidence. The fitted partial spectra for Si and O are also shown.

14.3.2 Databases implemented

One of the main conclusions of the IAEA intercomparison exercise of IBA softwares was that the greatest differences in the results arise from differences in the fundamental databases used, namely, the stopping-power database, as well as the non-Rutherford database in the case of EBS, ERDA, and NRA.

In the past decade, important advances have been made in terms of both new and more accurate experimental data and new theoretical and semiempirical schemes. Which databases are included in each code, as well as the possibility of loading new values, is thus an important factor.

14.3.2.1 Stopping power

The greatest advances in the knowledge of stopping power achieved in the past decade were for heavy ions. This was possible because of a wealth of new experimental data becoming available, which was integrated, for example, into both the most widely used stopping-power semiempirical interpolating scheme used in IBA work, SRIM (Ziegler, 2004; Ziegler *et al.*, 2008), and MSTAR (Paul and Schinner, 2001, 2002), a program that calculates stopping powers for heavy ions. See Chapter 2 for further information on computer calculations of stopping powers.

For instance, in Fig. 14.5, we show the calculated spectrum for a 3 MeV ${}^7\text{Li}$ beam impinging normally on a Si/SiO₂ (2×10^{18} at./cm²)/Ti (1.5×10^{18} at./cm²) sample and detected at 160°, as obtained using 1985 stopping-power values and SRIM version 2006.02. It is clear that the very large changes in the simulation will be reflected in the accuracy of analyses of real data, with errors of up to 10% being made in thickness values, depending on the stopping values used.

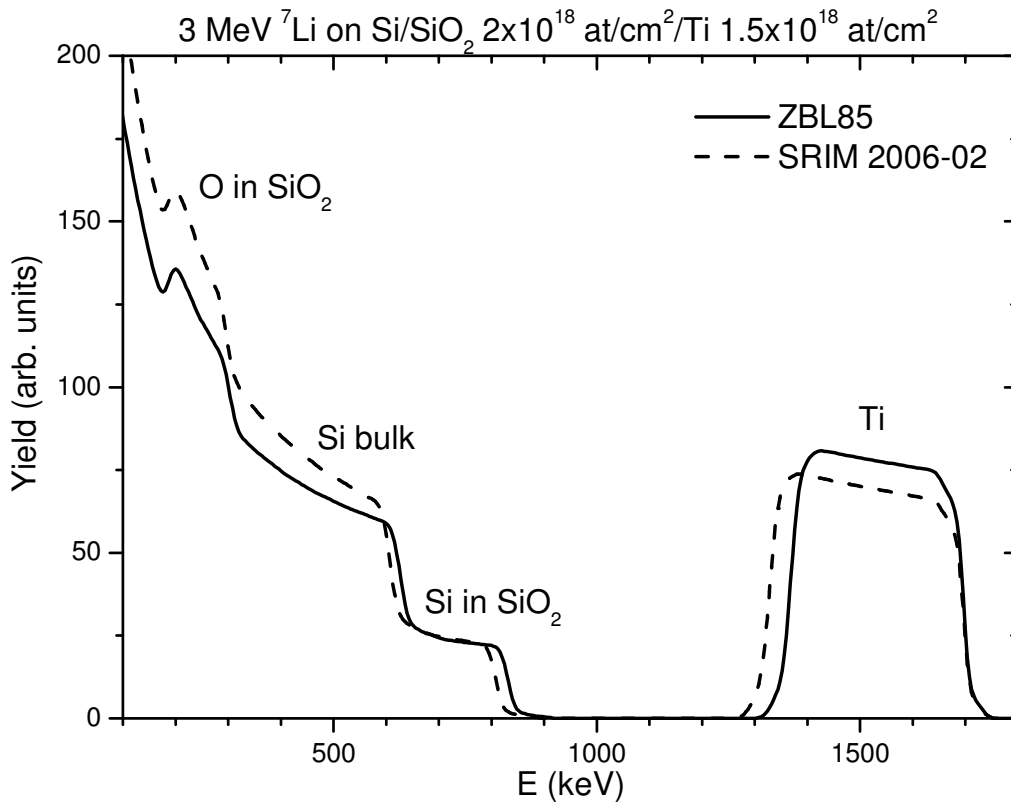


FIG. 14.5. Calculated spectra for 3 MeV ${}^7\text{Li}$ beam incident on a Si/SiO₂ sample. The only difference between the simulations is that different stopping powers were used: values from 1985 (solid line) and the most recently available values (dashed line). for accurate analyses, users must be aware of the stopping powers used by data analysis codes.

Large changes also occurred for light ions in some common systems. For instance, the stopping of He in Si is now known with an accuracy of better than 2%, and this update has been integrated into SRIM and other databases.

Also, many experiments in insulating compounds have shown that the Bragg rule does not always reproduce the experimental stopping, and the capability of including molecular stopping powers in codes is very important.

The stopping power along crystalline directions is usually smaller than that in a random direction or in an amorphous material with the same composition.

Ideally, codes should include the most recent stopping-power databases available, as well as the possibility of loading new stopping values for particular systems. In any

case, the users of data analysis software must be aware of the stopping used in a given analysis, along with its implications for the accuracy of the results obtained.

14.3.2.2 Scattering cross section

When analyzing EBS or NRA data, or ^4He ERDA measurements of hydrogen isotopes, for example, the non-Rutherford cross section used is of paramount importance. Some codes, namely SIMNRA, include a wide database of cross-section values for given ion/target pairs, whereas others read in external data files with the required cross sections.

The code SigmaCalc (Gurbich, 1997, 1998, 2005) for calculating cross sections from tabulated theoretical model parameters was developed by A. Gurbich. SigmaCalc is usually very reliable for those ion/target pairs that it includes, and it allows one to interpolate for scattering angles for which no measured cross sections are available. This action has also led to the integration of NRABASE and SIGMABASE into a single database called IBANDL (Ion Beam Analysis Nuclear Data Library), under the auspices of the IAEA.

Data with slowly changing non-Rutherford cross sections can be analyzed manually, as shown, for instance, in Chapter 5, section 5.3.4 of the first edition of this handbook (Tesmer and Nastasi, 1995) for ^4He ERDA analysis of hydrogen in $\text{Si}_3\text{N}_4(\text{H})$. However, this is a painstaking procedure that can be done much faster, and more accurately, by computer simulation.

When superimposed signals with fast-changing cross sections are present, it becomes almost impossible to analyze the data manually, and computer codes must be used, along with the appropriate cross sections. For example, in Fig. 14.6, we show 1.75 MeV ^1H backscattering off a TaNiC film on Si (Jeynes *et al.*, 2000b). The C signal is superimposed on the Si background, and both signals change rapidly because of the presence of resonances in both cross sections. The simulation includes one single homogeneous TaNiC layer and is the result of an automated fit that took less than 1 min. The scattering cross sections for C and Si were taken from SigmaCalc, and those for Ta and Ni are screened Rutherford cross sections.

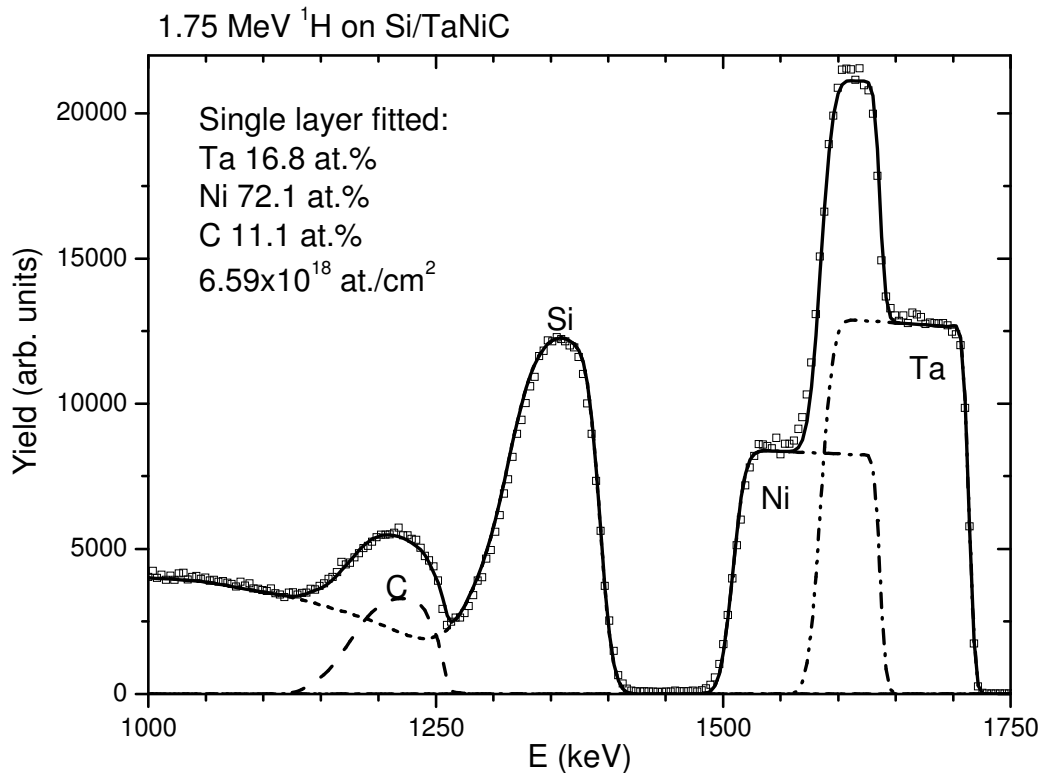


FIG. 14.6. Spectrum for 1.75 MeV ^1H backscattering off a TaNiC film on Si.

14.3.3 Basic physics

All IBA codes (except the Monte Carlo ones) employ similar principles to perform a basic simulation. The ingoing beam follows a straight trajectory, while losing energy, toward the sample; it interacts with a target nucleus; and the outgoing beam follows a straight trajectory, while losing energy, on its way to the detector. The energy spread of the beam (often called straggling) is also calculated.

From the point of view of the user, the fact that the different codes implement these steps in very different ways is not important.

The user wants to know, first, that all codes perform good simulations (at least for simple everyday spectra; complex samples might require particular codes). Confirming that a code is correct would imply a deep analysis of the physics included and of its implementation in the algorithms employed. Users do not want to do this, and often, they cannot (either because the source code is not available or because they do not have the time or the necessary background). Until recently, users simply assumed that codes were correct.

The IAEA intercomparison exercise showed that all of the analyzed codes produced similar results for a 1.5 MeV ^4He RBS simulation of a simple sample. Signal total yields and signal heights were calculated with a 0.1–0.2% standard deviation between codes (as long as the same stopping powers and scattering cross sections were used in all cases). This is thus the error due to the differences in implementation of the same physics. It is smaller than the typical experimental errors coming, for example, from

counting statistics (rarely better than 1%) and much smaller than the error in the stopping-power values.

With the assurance that the codes (at least those that participated in the IAEA intercomparison) are correct for simple cases, the user might be concerned with how fast the simulations are. With modern computers, the simulation of simple spectra, even with straggling included, is always fast. Efficiency becomes important only when some further physics, such as plural scattering, is included.

14.3.4 Advanced physics

Although all simulation codes treat basic ion stopping and scattering phenomena, many of the subtle features in spectra arise from more complex interactions. The main issues involve energy spread, multiple and plural scattering, the handling of non-Rutherford cross sections, surface and interface roughness, and channeling.

The first comment is that, in principle, the best way of dealing with all of these phenomena is full Monte Carlo simulations. MCERD, for instance, is a Monte Carlo code for the analysis of ERDA data, but it can also handle RBS. It can include all of these effects, except for channeling. Different codes have been dedicated to the analysis of channeling in specific systems.

However, MC codes are mostly used by their authors, and calculation times can be an issue. Development of intuitive user interfaces and continuing gains in efficiency might change this situation, but for the moment, traditional codes are still the most often used. The following discussion is therefore related to traditional codes

We are concerned with determining the situations in which the basic simulations discussed in Section 14.3.3 are adequate. In situations where they are not adequate, we want to know whether codes include enough further physics to lead to meaningful analysis. The capabilities of the different codes are summarized in Table 14.7.

14.3.4.1 Straggling models

Practically all of the IBA codes implement the Bohr model (Bohr, 1948); with or without the Chu/Yang correction (Chu, 1976; Yang *et al.*, 1991), important for He and heavier beams; some also implement the Tschalär effect (Tschalär, 1968a, 1968b; Tschalär and Maccabee, 1970), which is important in thick layers (for instance, to calculate the energy spread in a buried layer or after a stopper foil). Some codes let the user scale the calculated straggling. We note that pure Bohr straggling (without the Tschalär effect) is valid in a rather narrow range of energy loss, typically when the energy loss does not exceed around 20% of the initial beam energy.

However, straggling is important only if the detailed signal shape carries relevant information. To determine the stoichiometry and thickness of films, straggling is very often irrelevant, and the user can either ignore it or adjust the straggling to match observed signal widths. In this case, all codes are adequate.

If, on the other hand, interdiffusion or roughness between layers is being studied, or if a changing depth profile must be derived with maximum achievable accuracy, then any error in the straggling will directly lead to an error in the results. In such situations, the best available theory (i.e., a code that implements it) must be used.

State-of-the-art calculations of straggling, including geometrical straggling and multiple scattering, are performed by the code DEPTH (Szilágyi *et al.*, 1995; Szilágyi, 2000). The recently presented RESOLNRA code (Mayer 2008) leads to equivalent results.

No code dedicated to general-purpose IBA data analysis implements accurate straggling functions such as the Landau–Vavilov function. See, for instance, Bichsel (2006) and references therein for a detailed discussion of this issue.

The codes NDF and SIMNRA implement or are developing asymmetric straggling functions that might not be physically correct but that do represent reality better than the usual Gaussian distributions.

14.3.4.2 Electron screening

Electron screening at low energies decreases the effective charge of the target nucleus seen by the analyzing ion, leading to a smaller scattering cross section (L'Ecuyer *et al.*, 1979; Andersen *et al.*, 1980). It is greater for heavier target species and heavier ions, as well as for lower energies. For 1.5 MeV ^4He RBS off gold, it leads to a 2% correction to the cross section. Most codes implement this effect.

14.3.4.3 Plural scattering

Plural scattering involves a few large-angle scattering events. It leads to a low-energy background, to an increased yield of bulk signals at low energies, and potentially to yield above the surface energy. Plural scattering can normally be disregarded, even when it is sizable, because it changes slowly with energy, and *ad hoc* backgrounds or signal subtraction techniques are often used.

Plural scattering is important on the rare occasions where the yield at low energies or in a given background region must be understood quantitatively. Also, at grazing angle (of incidence or detection), it can make a large contribution even to the signal of fairly thin surface films. Both SIMNRA (Eckstein and Mayer, 1999) and NDF (Barradas, 2004) can calculate double scattering (two large-angle events, which accounts for most plural scattering). The two algorithms are not equivalent, but they lead to similar results in most situations. In some cases, such as in grazing-angle geometries, large differences might be observed, so the user should study the respective literature. Calculations are slow and not as accurate as for single scattering, but excellent reproduction of observed signals can be obtained, as seen in Fig. 14.7 (Mayer, 2002) for a normal incidence spectrum.

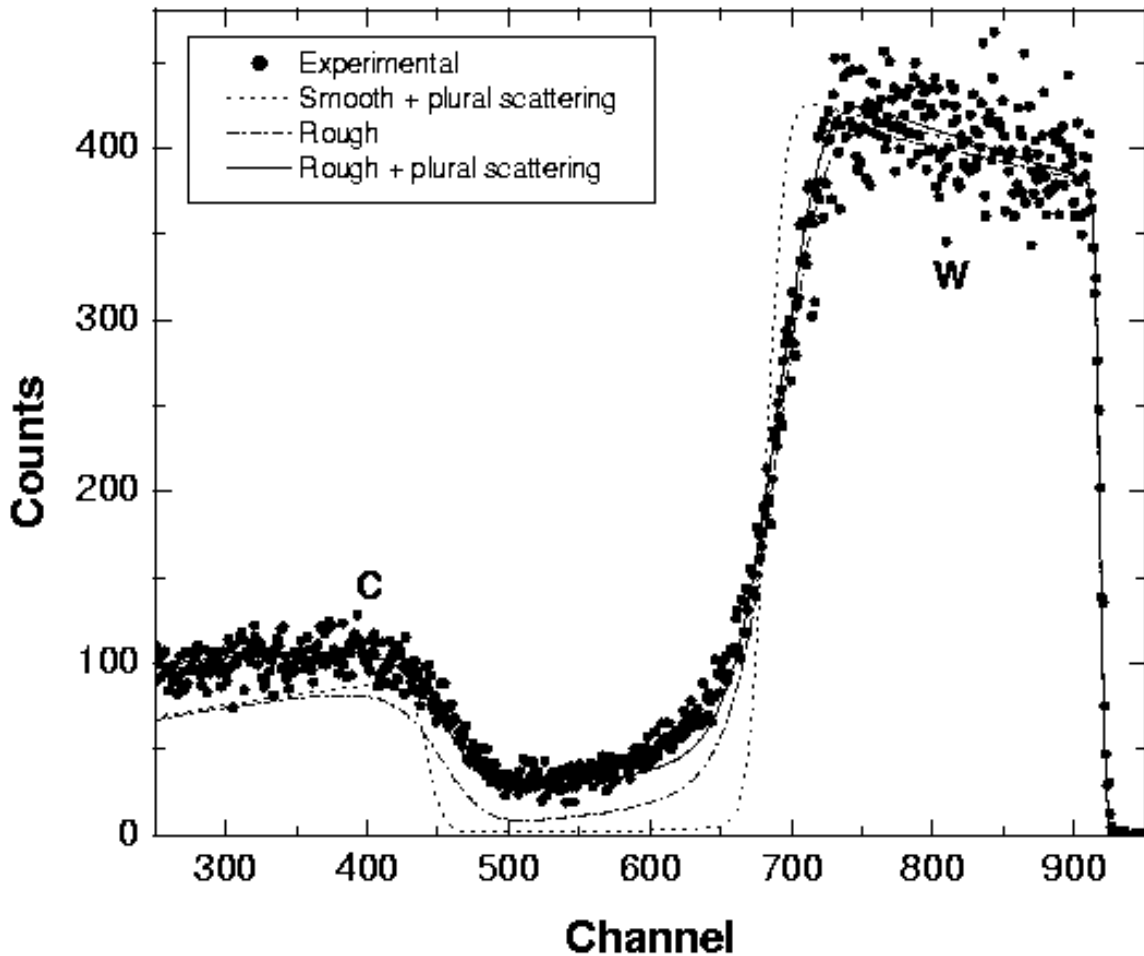


FIG. 14.7. 2.5 MeV protons backscattered from a 3.5- μm W layer on a rough carbon substrate, at normal incidence and with a scattering angle 165° . (Circles) Experimental data, (dotted line) calculated spectrum for a smooth W layer (3.6 μm) on a smooth C substrate including plural scattering, (dashed line) calculated spectrum for a rough W layer (3.5 μm , $\sigma = 0.30 \mu\text{m}$) on a rough substrate (fwhm 20°); (solid line) same as dashed line but including plural scattering. (From Mayer, 2002.).

14.3.4.4 Multiple scattering

Multiple scattering involves a large number of low-angle scattering events. It changes the trajectories of the beam ions, making them quite different from straight lines. This has many consequences, some of which standard codes are unable to calculate. It is therefore critical to know when it is important and when its effects can be calculated adequately.

Multiple scattering leads to an extra contribution to the energy spread of the beam, a change in the shape of signals because this contribution is not Gaussian-shaped, and a change in the observed yield.

It is more important for heavier ions at lower energies in heavier targets, as well as for grazing angles. In fact, at near-normal incidence, for the detection of ions with energies in the typical IBA range, multiple scattering can almost always be ignored.

At grazing angles (for instance, in ERDA), multiple scattering is often the most important contribution to energy spread. If energy spread is important (see Section 14.3.4.1), then multiple scattering must be calculated.

The best available calculations of multiple scattering (but not necessarily the best simulation of energy spectra) are made by the code DEPTH (Szilágyi *et al.*, 1995). Some codes implement the extra energy spread, but assume it to be Gaussian-shaped. Most codes do not calculate multiple scattering. For heavy ions at fairly low velocities in grazing-angle geometries, none of the standard codes compares very well with Monte Carlo calculations, as of the time this was written.

14.3.4.5 Simulation of resonances

It is quite difficult to simulate buried sharp resonances. The combination of “buried” and “sharp” means whenever the energy spread of the beam before scattering is comparable to the resonance width. For bulk signals, the shape of the resonance signal is considerably affected; for thin films, the actual yield is also affected. This is important whenever a sharp resonance is used to enhance the yield from a buried element.

For instance, for protons crossing a 4.2- μm Ni film (leading to a high energy spread) on top of a 1- μm Mylar film, the calculated C yield from the Mylar can be wrong by a factor of 10 if the energy spread of the beam is not taken into account (see Fig. 10 of Barradas *et al.*, 2006).

To the best of our knowledge, the only code for analysis of general RBS and ERDA data that is currently able to calculate correctly the shape and yield in the presence of buried sharp resonances is NDF (Barradas *et al.*, 2006). Dedicated codes for specific systems (Tosaki *et al.*, 2000) and for resonant NRA (Vickridge and Amsel, 1990; Pezzi *et al.*, 2005) also exist.

14.3.4.6 Surface and interface roughness

There is no general definition of roughness. Many different types of roughness exist. In the context of IBA, the most important point is that, in general, RBS experiments are not sufficient to determine which type of roughness is present. In fact, they are not even capable of distinguishing between layer interdiffusion and interfacial roughness. In almost all cases, extra information from other techniques [usually transmission electron microscopy (TEM) or atomic force microscopy (AFM)] is required. That said, RBS can be very useful for quantifying roughness in some cases.

Several methods exist to simulate spectra including roughness. The most accurate is to perform a Monte Carlo simulation, modeling the desired surface or interface. In general, roughness is not amenable to routine data analysis.

A typical approach in analytic codes is to sum partial spectra over a distribution function of some sample characteristics, such as surface height or film thickness. RUMP and SIMNRA implement different variations of this method.

A second approach is to calculate analytically the effect on signal width due to a given type of roughness and to take the result as an extra contribution to energy spread. In this approach, spectra can be calculated in the usual way. NDF implements this method, which has stringent but well-defined conditions of applicability, for different types of roughness and also for inclusions, voids, and quantum dots. Both approaches ignore

correlation effects and fail for features with large aspect ratios leading to re-entrant beams.

An analysis of a rough sample performed using SIMNRA is shown in Fig. 14.7 (Mayer, 2002), where plural scattering also plays an important role. The sample is a rough W layer on a rough C substrate, which is a very complex situation. Quantitative information on the roughness parameters is obtained in a relatively simple way, as the user needs only to specify the type and amount of roughness and the code takes care of all of the calculations.

A new algorithm to take correlation effects and re-entrant beams into account was recently published (Molodtsov *et al.*, 2009). It is, strictly speaking, for the published formulation, valid only for single-layer targets, but once it is included in data analysis codes, it will expand the range of samples that can be meaningfully analyzed.

14.3.4.7 Channeling

Specific methods have been developed to analyze channeling data. Most standard analytic codes are simply not capable of analyzing channeling. Some implement *ad hoc* corrections to the channeled yield in order to be able to derive information from unchanneled parts of the spectrum. Only one of the standard codes that participated in the IAEA intercomparison exercise, RBX, is actually capable of simulating the channeled RBS spectra of virgin crystals, even with point defect distributions.

14.3.4.8 Pulse pileup

Pileup leads to some counts being lost and some counts being gained in the collected spectrum. Without exception, more counts are lost than gained, and so the total yield, integrated over the entire energy range, is smaller than it would be for a perfect detection system.

Some codes calculate pileup based on system parameters such as amplifier type, amplifier shaping time, beam current, collection time, and characteristic time of a pileup rejection circuit if present (Wielopolski and Gardner, 1976, 1977; Gardner and Wielopolski, 1977; Molodtsov and Gurbich, 2009). This can be important in some cases, particularly given that pileup is not linear and can be a correction of several percentage points to the yield. It should always be calculated, except for very low count rates. Chapter 15, Pitfalls in Ion Beam Analysis, describes an example.

14.3.5 Automated optimization

Practically all codes can work interactively. The user examines the data, makes an initial guess of the sample structure, calculates the corresponding theoretical spectrum, and compares it to the data. Differences drive modifications in the defined structure until the user considers the agreement to be adequate (or, rather often, until patience runs out).

In automated optimization, it is the computer code that controls this procedure. Users should be aware that an objective criterion of goodness of fit is needed, usually a χ^2 or likelihood function. It is this function that the codes try to optimize. This can lead to a serious pitfall. If the model does not describe all of the relevant physics (for instance, if multiple scattering is important but not calculated or calculated poorly) or if the user introduces too few or too many elements in the sample description, a good fit that also corresponds to the true sample structure cannot be obtained. The code will output

something, but what it outputs will not be a good solution. We cannot overemphasize the fact that automated optimization is a wonderful feature, but it can lead to substantial errors unless great care is taken in checking the results.

If several spectra were collected, the possibility of fitting them all simultaneously, with the same sample structure, is essential to ensure that the results are consistent and that all of the information present in the spectra is taken into account to generate the final result.

14.3.5.1 Fitting

Automated fitting is designed to relieve the user from this task. Not all codes do it. Some, such as RUMP and SIMNRA, perform a local optimization on a limited number of parameters, starting from an initial guess that usually must include the correct number of layers.

NDF uses an advanced algorithm, simulated annealing (Kirkpatrick *et al.*, 1983), complemented by a local search, to find an optimum solution without any need for an initial guess, except for the elements present. All parameters can be fitted.

14.3.5.2 Bayesian inference

IBA is often fully quantitative without needing standards. This is arguably its greatest strength. However, actual error bars or confidence limits on the concentrations, thickness values, and depth profiles determined are almost never presented or published. This is arguably the greatest weakness of IBA work.

In the past decade, Bayesian inference (BI) methods have been applied to IBA data analysis, providing a tool to systematically determine confidence limits on the results obtained (Barradas *et al.*, 1999; Padayachee *et al.*, 2001; Neumaier *et al.*, 2001; Mayer *et al.*, 2005; and Edelmann *et al.*, 2005). The mathematics is somewhat involved, but the users of codes do not need to be concerned with the details.

In practical terms, instead of producing one best fit, for instance, minimizing the χ^2 , BI performs a series of simulations, for very many different sample structures and depth profiles, all of which are consistent with the data. Statistical moments, such as the average and standard deviation, can then be calculated.

During the BI calculations, the known experimental errors, including those in the energy calibration, solid angle, beam fluence, and even beam energy or scattering angle, can be introduced. These errors, together with the statistical counting error, are then reflected in the final error calculated for the depth profile.

The codes MCERD and NDF both implement BI. It is computationally expensive; that is, it takes much longer to perform a BI run than to do a least-squares fit. For the moment, BI is still not suitable for the routine analysis of large amounts of data. A few samples per day can be analyzed, however, and BI is the only method that can provide reliable error bars in a general way.

14.3.6 Usability and usage

Usability of a code refers to how easy it is to use the code correctly. This depends on how intuitive and simple the user interface is, but also on how much knowledge the user has about the technique used. Nonexpert users might not know that scaling a given stopping power by a factor of 2 might not be justifiable or that intermixing and surface

roughness can have the same effect on measured data. Many other examples can easily be found by carefully reading published work, where inaccurate or wrong results due to bad data analysis are unfortunately not uncommon.

The easiest code to use is often considered to be RUMP, whether in its command-line or windowed incarnations, and no chapter on IBA software could go without citing its “beam me up Scottie” command line (see EXAMPLE 14.3). First-generation codes such as GISA already included strong graphical capabilities and easy-to-navigate menus. RBX allows quick editing of parameters for analysis of multiple spectra.

The new-generation codes have more user options and, as a consequence, are perhaps not as intuitive. To use advanced physics features, one often must have knowledge of the issues involved and of an increased number of system parameters. As a consequence, usage (particularly by novices) is more prone to errors. SIMNRA is considered easier to use than NDF. Their manuals state they are “easy to use” (Mayer, 2007) and “designed to be a powerful tool for experienced analysts of Ion Beam Analysis data” (Jeynes *et al.*, 2000c), respectively. MC codes such as MCERD are not yet widely used except by the authors and their collaborators. This might change soon as one of the MC codes, Corteo, now has a user-friendly windowed interface (Schiettekatte, 2008).

The IAEA intercomparison exercise originally planned to test usability by novices and expert users, but this has not yet been done.

RUMP is historically the most-cited IBA data analysis code, with around 120–150 citations per year in the past decade. SIMNRA came a close second in 2007, and if the trend continues, it will overtake RUMP as this book is being published. NDF, the third most cited code, receives about one-half the citations that SIMNRA does. SIMNRA and NDF combined now account for more citations than RUMP does. Citations might be misleading when trying to assess real use of a code, however, as users might not always cite the code they use.

14.4 ACCURACY

The accuracy that can be achieved in an IBA experiment depends on many parameters. For each given experiment, an uncertainty budget can be made, including all of the different sources of error. A detailed example of uncertainty estimation is provided in Chapter 15, Pitfalls in Ion Beam Analysis.

Data analysis codes cannot lead to results that are more accurate than the models applied and experimental data analyzed. Furthermore, most of the codes usually do not produce an error analysis, just numbers without associated accuracies. The consequence is that it is almost universal practice to quote the results provided by the codes, such as concentrations, layer thicknesses, or depth profiles, without quoting the associated uncertainties. Given that IBA techniques such as RBS and ERDA are inherently quantitative, this is not really justifiable.

Bayesian inference can be used as a means of error analysis (Barradas *et al.*, 1999), but it is not implemented in most codes, and it is computationally intensive. The uncertainty budget is a valid alternative, but it requires detailed knowledge that many users do not have.

14.4.1 Numerical accuracy of codes

The codes themselves have an associated accuracy. For exactly the same sample structure and experimental conditions and including exactly the same physics, no two codes will calculate numerically the same theoretical spectrum. Differences in implementations of the physics and algorithms and even in floating-point representation do lead to differences in the calculated spectra and, thus, to different final results of the data analysis. The issue is how large these differences are.

The codes that took part in the IAEA intercomparison exercise (Barradas *et al.*, 2007b) were compared numerically and validated. For ^4He RBS, differences of up to 0.2% were found. For ^7Li RBS, this increased to 0.7%. For ^4He ERDA, differences between 0.5% and 1.3% were found in calculated yield values. This is a further source of inaccuracy that should be included in the uncertainty budget. We note that experimental uncertainties down to about 0.5% are difficult to reach, but have been reported (Jeynes *et al.*, 2006; Barradas *et al.*, 2007b). This means that, at least for ERDA and heavy-ion RBS, the accuracy of the calculations can be an issue.

However, if we consider only the codes RUMP, NDF, and SIMNRA, which together account for over 80% of the citations in work published in 2006 and 2007, then the differences are 0.1% for ^4He RBS, 0.3% for ^7Li RBS, and 0.1% for ^4He ERDA. These results are significantly better than the achievable experimental uncertainty and much better than the uncertainty with which stopping powers are currently known.

14.4.2 Intrinsic accuracy of IBA experiments

The intrinsic accuracy of IBA experiments is limited by three main factors: the accuracy of the models applied and the related basic physical quantities, such as cross sections or stopping powers the accuracy with which the experimental parameters are known; and the counting statistics.

14.4.2.1 Models and basic physical quantities

Many different models are used in IBA data analysis to describe the various physical phenomena involved. The accuracy of these models is often difficult to assess. Examples are stopping and scattering cross sections, plural and multiple scattering, screening, the energy spread, the detector response, pileup, and so on. A few examples are briefly considered in this section.

The accuracy of scattering cross sections is limited at high energies by the occurrence of elastic nuclear reactions. In this case, experimental cross sections or cross sections evaluated with nuclear models must be used (see, e.g., IBANDL). The errors involved depend on the error of the cross-section measurements. Users interested in accuracy must check the original literature for each reaction, but accuracies better than 1–2% are almost never achieved, and 10% is common. Given that many cross sections have a strong angular dependence, the uncertainty in the scattering angle leads to an even larger error that is difficult to evaluate. Nuclear models can predict scattering at angles where experimental data are not available, and SigmaCalc should be used for all reactions where it is available at the required energy range.

In the low-energy limit, electron screening becomes the issue. For 1 MeV $^4\text{He}^+$ backscattered off Ta, the cross section is already 3% smaller than the Rutherford formula (Rauhala, 1987). For 0.3 MeV $^4\text{He}^+$ forward-scattered off Au at a 15° angle, the correction is about 33% (Andersen *et al.*, 1980). However, in both cases, this factor can be calculated, for instance, by the angular-dependent screening correction given by

Andersen *et al.* (1980), which leads to cross sections accurate within 1% for scattering angles above 15° and $^4\text{He}^+$ energies above 0.3 keV. For the typical velocities in RBS, the accuracy is not better than 0.2% for heavy target elements such as Au.

The limited accuracy of stopping powers is a fundamental limit to the accuracy with which layer thicknesses and depth profiles can be determined. A statistical analysis by Ziegler showed that the average standard deviation of SRIM-2003 stopping-power calculations relative to experimental values is 4.2% and 4.1% for H and He ions, respectively, and 5.1% and 6.1% for Li and heavier ions, respectively (Ziegler, 2004). For H and He ions, 25% of the calculations are off by more than 5% relative to the experimental values. For heavy ions, this increases to 42% of all SRIM stopping powers, and 18% of the calculations having an error larger than 10%. Very few stopping powers are known with an accuracy better than 2%.

For light compounds, particularly insulators, the Bragg rule can lead to large errors (above 10% at the stopping peak).

14.4.2.2 Experimental conditions

The experimental conditions, such as beam energy, incidence and scattering angles, beam fluence, solid angle of the detector, multichannel analyzer (MCA) energy calibration, and others, all have an associated accuracy, which is often not known. The reader is referred to Chapter 15, Pitfalls in Ion Beam Analysis, for a further discussion of this issue.

14.4.2.3 Counting statistics

Experiments cannot last indefinitely. Often, a limited amount of beam time is allocated for a given number of samples that must all be measured. More generally, counting statistics is limited by the damage caused to the sample by the beam. In any case, Poisson statistics (often approximated as Gaussian statistics) is well understood and is used in most error analyses that are actually published. One common example is to calculate the error of an isolated signal as the square root of the integrated yield. This leads to an underestimation of the true accuracy, which is often much worse than what would be granted only by statistics.

14.4.3 Physical effects on data analysis

The effects that some physical phenomena have on data analysis are described in Table 14.9. Where possible, the resulting errors were quantified. Note that the error values given are indicative only, and a detailed error analysis must be made on a case-by-case basis.

With this table in mind, the following advice can be given:

- Always include electron screening in the calculations. The angular dependence of screening is important at small scattering angles and low energies, so it should be included [in practice, this means Andersen *et al.* (1980) screening].
- For proton beams at any energy and ^4He beams at energies as low as 2.0 MeV, always check the literature and the IBANDL database for possible nuclear reactions and the corresponding cross sections.

- Always use the most recent stopping-power data available. In some cases, particularly for heavy ions, this can imply using literature values and not one of the popular interpolative schemes.
- Be aware of the accuracy with which you know the experimental parameters. The nominal values cannot be taken for granted unless a strong effort has been made to determine them.

Furthermore, depending on the experiment at hand, the following points might need to be included in the analysis:

- One of the sources of the low-energy background is double scattering. If an accurate low-energy calculation is important, then use a code that can calculate double scattering. However, other sources, such as slit scattering, also lead to similar backgrounds and might be impossible to calculate.
- Calculate pileup whenever the count rate is not very low or whenever a high-energy background is observed.
- All contributions to energy spread, including geometrical straggling and multiple scattering, must be calculated whenever the broadness of signals is relevant to the analysis.
- Calculate the effect of surface and interface roughness whenever relevant; very often, surface roughness is ignored and falsely assigned to layer intermixing.
- Read carefully Section 14.3.4 (Advanced physics) and Section 14.6.1 (Further capabilities), some of the issues discussed might be relevant to the analysis of your data.
- Read carefully Chapter 15 of this handbook, Pitfalls in Ion Beam Analysis, particularly the sections on accuracy and the error budget.

14.5 RUMP AND FIRST-GENERATION CODES

In 1976, Ziegler and co-workers published the first code, called IBA, that performed full simulations of RBS spectra (Ziegler *et al.*, 1976). In the next decade, a series of codes surfaced, the most popular of which was RUMP (Doolittle, 1985).

Many versions of RUMP are available, including some very early ones. Users are cautioned that they should regularly download the new version (along with the companion code Genplot): RUMP is being actively developed, and new versions incorporate such updates as recent stopping powers, heavy ions, and improved algorithms.

RUMP is very reliable for what it is designed to do. This fact, together with its being easy to learn and use, is the main reason for its popularity. Novice users can obtain accurate results from simple spectra without too much work. In the RUMP example (EXAMPLE 14.3), we show how information can be extracted from a fairly complex spectrum by an expert user. This is one of the samples that was analyzed in the IAEA intercomparison exercise of IBA software.

EXAMPLE 14.3. RUMP.

In this example, sample E3 from the IAEA intercomparison exercise of IBA software (Barradas *et al.*, 2007b) is used. It is a hafnium oxide layer with impurities on a Si

substrate, analysed by RBS with a 2.5 MeV $^4\text{He}^+$ beam. The first step is to load the data and define the experimental conditions. This is done in RUMP by using an edit window or by commands given in the best known screen in IBA (Fig. 14.8).

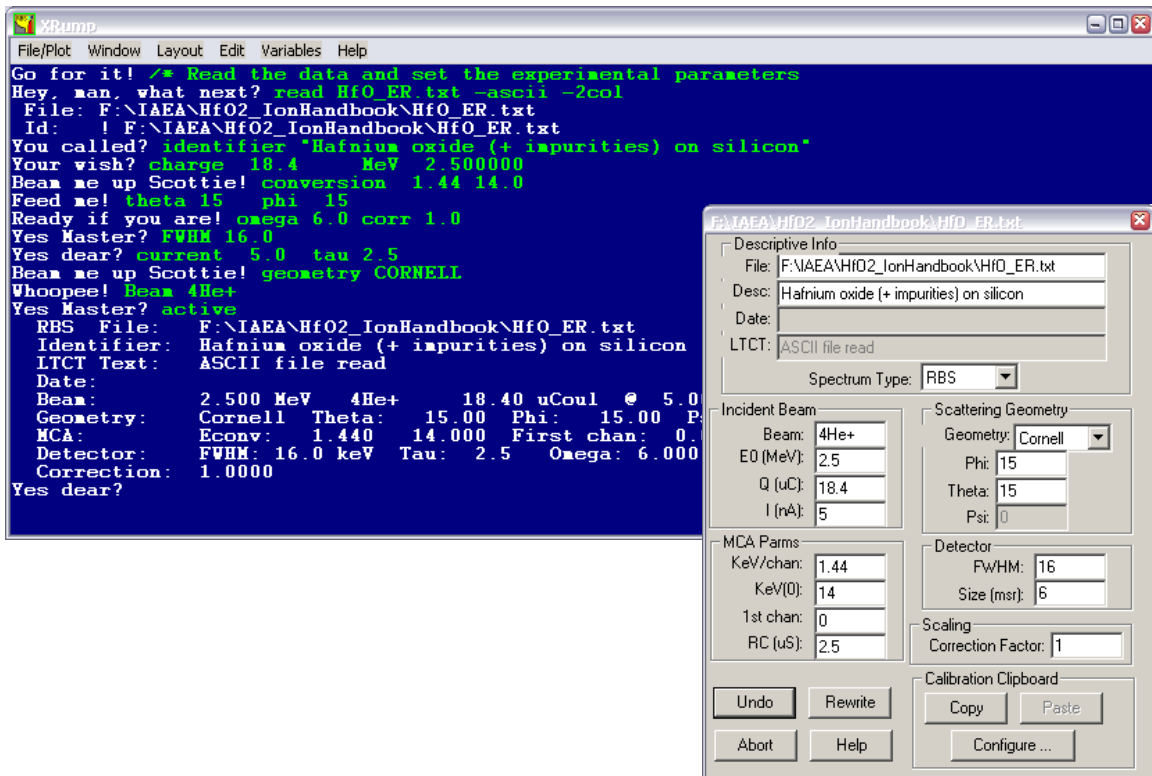


FIG. 14.8. First step of a RUMP analysis: load the data and define the experimental conditions.

The second step is often to configure some simulation parameters using line commands. In this case, SRIM-2006 stopping powers are used, the non-Rutherford scattering cross section for the $^{16}\text{O}(\alpha,\alpha)^{16}\text{O}$ is loaded, and straggling and multiple scattering are enabled. By default, all isotopes are calculated separately (as opposed to making one single calculation for the average mass of the target element), and Andersen electron screening (Andersen *et al.*, 1980) is included.

```
XRump
File/Plot Window Layout Edit Variables Help
You called? /* Configure options
Your wish? pen -1 linewidth 2 /* Plot options
Yes dear? linetype 0 symbol OpenCircle symSize 0.05
Your wish?
Next? config user_stop zb106 /* SRIM 2006 stopping
MSG: ZStop() from C:\Program Files\cgs\RUMP\NT\Local\zb106.dll will be used for
stopping power
Configuration subcommand: sim
SIM Command: resread oxygen_resonance_15deg.adt /* Oxygen resonance
Resonance data: z1=2 m1=4 z2=8 m2=16 phi= 15.00 npt=245
SIM Command: straggle 1 /* Enable straggle
SIM Command: multiple_scatter 1 /* Enable ad-hoc multiple
SIM Command: region 0 2000 sqrt
Yes dear? |
```

FIG. 14.9. Second step of a RUMP analysis: Configure simulation parameters.

The third step is to define the sample structure. This is done using intuitive, easy-to-learn commands. The corresponding first guess is then calculated.

```

XRump
File/Plot Window Layout Edit Variables Help
Your wish? sim
SIM Command: layer 1 comp Hf 1.0 Zr 0.010 O 2 / thick 1000 /cm2
SIM Command: layer 2 comp Si 1 / thick 3 um
SIM Command: show
# Thickness Sublayers Composition
1 1000.00 /CM2 auto Hf 1.000 Zr 0.010
O 2.000
* 2 3.00 um auto Si 1.000
-----
SIM Command: return
Yes Master? plot 1 overlay theory -lt 1
Automatic simulation . fwhm(0.000) . pileup(0.010) . all(0.080) . performed.
Your wish? sim
SIM Command: multiple 1.15 /* Manually match multiple scattering
SIM Command: plot 1 overlay theory -lt 1
Automatic simulation . fwhm(0.000) . pileup(0.010) . all(0.080) . performed.
Here I am!

```

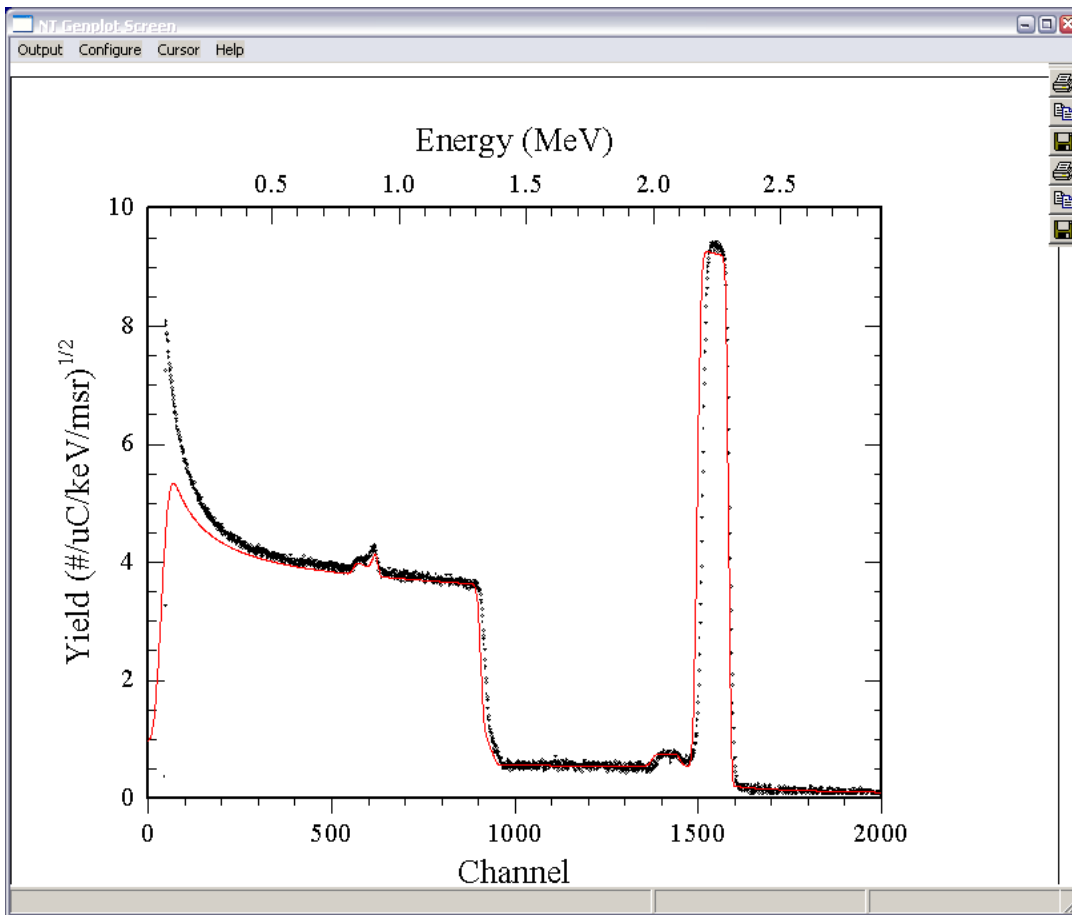


FIG. 14.10. Third step of a RUMP analysis: define the sample structure, perform the simulation.

A manual iterative procedure as described in EXAMPLE 14.1 would follow the first guess. Alternatively, RUMP includes an optimization algorithm. The window shows the definition of the fitting space and the final results. In most situations, not all variables would be fitted at the same time. A combination of manual iterations and fitting of some parameters is typical.

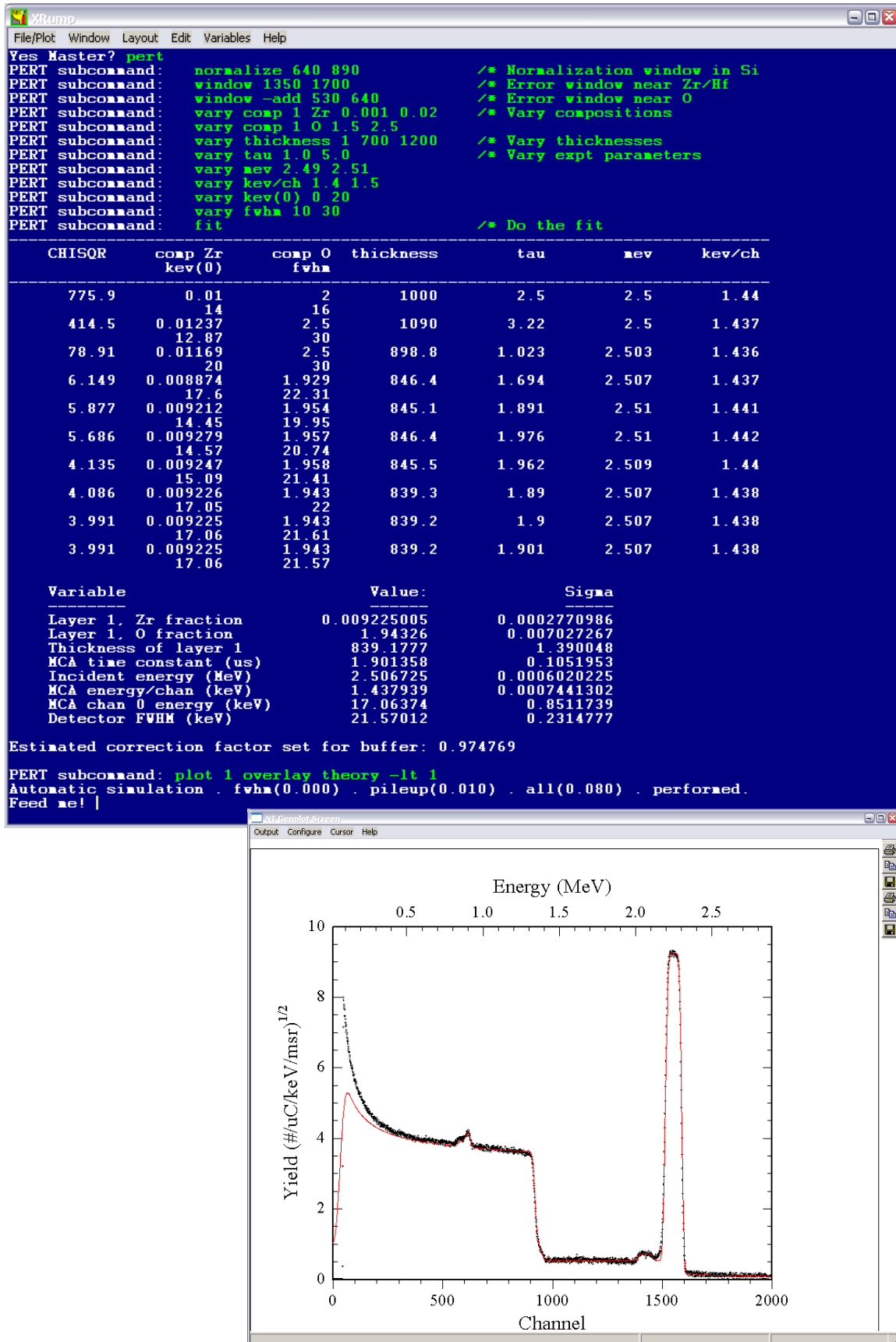


FIG. 14.11. Final result of a RUMP analysis after manual or automated iteration until agreement between simulation and fit is achieved.

However, the IBA samples that need to be analyzed are becoming increasingly complex, making stronger demands on data analysis. Advanced physical effects such as roughness, quantum dots and inclusions, and multiple and plural scattering, as well as simultaneous use of multiple techniques or different experimental conditions, need to be included in routine data analysis.

RUMP lacks many of these capabilities, which is probably the reason why new-generation codes such as SIMNRA are overtaking it.

Other popular first-generation codes, used by different groups (as opposed to the many codes that are used mostly by their author only), are GISA (Rauhala, 1984; Saarilahti and Rauhala, 1992) and RBX (Kótai, 1994), which places strong emphasis on working with sets of spectra from the same sample.

14.6 NEW-GENERATION CODES: SIMNRA AND NDF

Several IBA data analysis codes were developed in the 1990s. Of these, SIMNRA (Mayer, 1997) and NDF (also known as DataFurnace) (Jeynes *et al.*, 2003) placed strong emphasis on implementing advanced physics and experimental conditions.

Another code, DEPTH (Szilágyi *et al.*, 1995), was developed specifically to make state-of-the-art calculations of depth resolution. It is not geared toward the analysis of data, but it (or a different implementation of the same algorithms) should be used whenever depth resolution is important.

14.6.1 Further capabilities

The reader is referred to Section 14.3 for information about when the effects mentioned in this section are important.

SIMNRA and NDF both implement plural and multiple scattering effects to some extent. Multiple scattering is included only insofar as it affects the depth resolution.

SIMNRA includes its own algorithms to calculate the depth resolution. NDF uses a different approach, which is to call DEPTH in run time (NDF writes the required input files automatically) and use the DEPTH results. This has the advantage that DEPTH is the state of the art in terms of depth resolution and is still being developed and updated, and it has the disadvantage that the user must also have DEPTH (which is free of charge) installed.

Both codes have some roughness capabilities. SIMNRA calculates very many different trajectories for actual surfaces, as defined by the user. This approach is accurate, and slow, and it requires detailed knowledge of the sample surface. NDF uses models for a few types of roughness, as well as for inclusions and quantum dots. This approach is fast and requires less knowledge by the user, but it is not as accurate. In practice, the SIMNRA approach is best for detailed studies of a few very important samples, whereas the NDF approach is adequate for routine analysis of roughness parameters.

SIMNRA includes RBS, ERDA, and nonresonant NRA for any ion detected at any angle (including forward scattering and transmission) and for any target. NDF includes those techniques, as well as PIXE (Pascual-Izarra, 2006a) and resonant NRA.

SIMNRA offers some limited support for multiple spectra collected from the same sample. The user must write a script or small program and use OLE (object linking and embedding) automation, supported by SIMNRA. NDF is designed for analyzing any number of spectra from the same sample. The same depth profile is used to fit all of the spectra simultaneously. There are no restrictions on using data from different techniques, and all complementary information is integrated into the final result.

Barradas and co-workers published algorithms to improve the simulation of buried resonances (Barradas *et al.*, 2006), double scattering at grazing angles (Barradas, 2004), the yield at very low energies (Barradas, 2007), and the shape of surface signals in high-resolution experiments (Barradas *et al.*, 2007a). As of the time of publication of this handbook, these effects are included only in NDF, but other codes can easily include them as well.

14.6.2 SIMNRA

Development of SIMNRA started in 1996. It is a Windows code with intuitive menus and windows.

We show in the SIMNRA example (EXAMPLE 14.4) exactly the same spectrum as was used for the RUMP example (EXAMPLE 14.3). It is easy to follow how a rather different procedure leads to equivalent results.

EXAMPLE 14.4. SIMNRA.

In this example, sample E3 from the IAEA intercomparison exercise of IBA software (Barradas *et al.*, 2007b) is used. It is a hafnium oxide layer with impurities on a Si substrate, analysed by RBS with a 2.5 MeV $^4\text{He}^+$ beam. The first step of the analysis, after loading in the data, is to define the experimental conditions. This is done in an intuitive windows called from the Setup menu. In the example shown, the real and live times are used to apply a live-time correction and to calculate the pileup contribution. The final result of the analysis is already shown here; in a situation where analysis is just starting, only the data would appear.

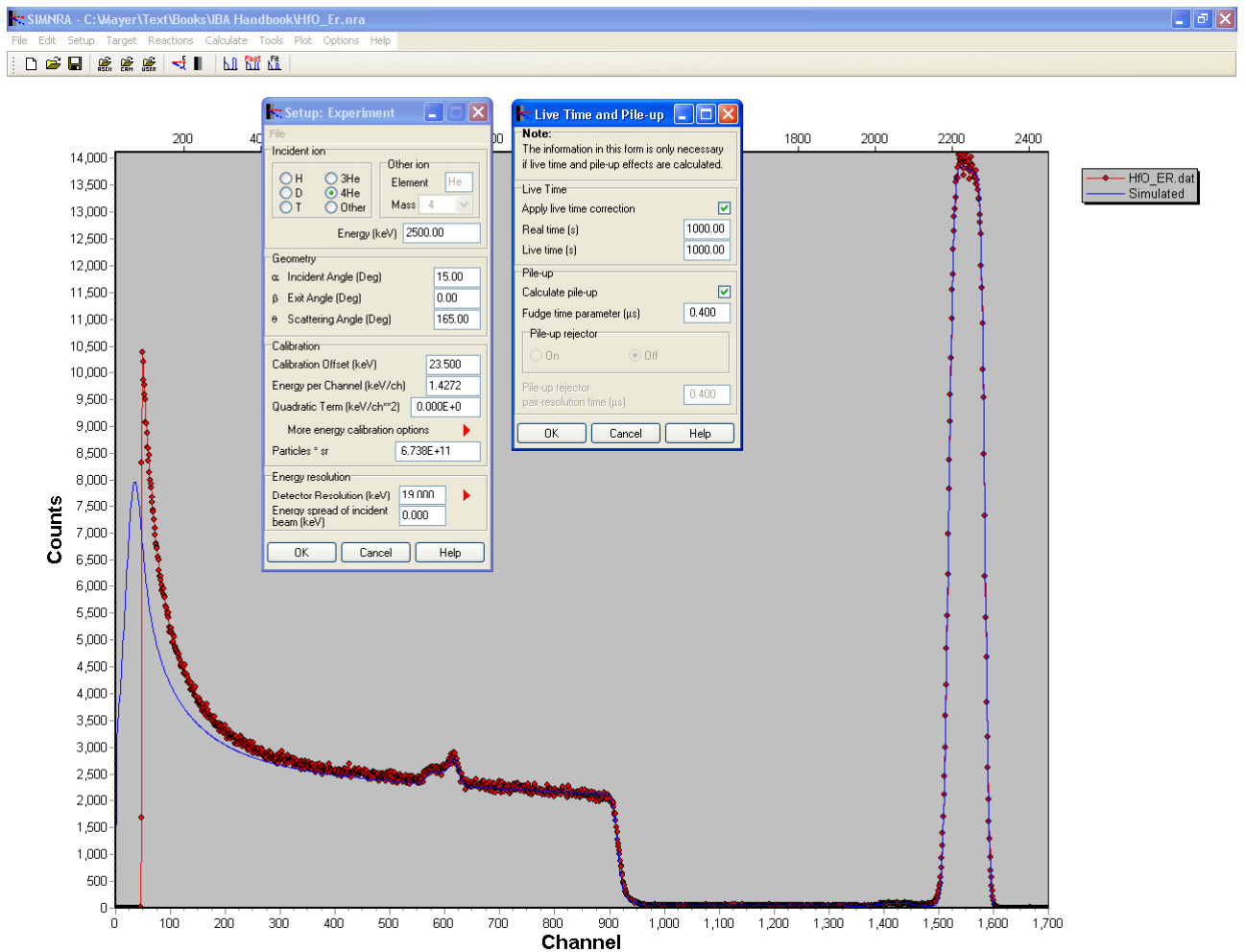


FIG. 14.12. First step of a SIMNRA analysis: load the data and define the experimental conditions.

The second step is to define the physics included in the calculation. In this case, all isotopes are calculated separately (as opposed to making one single calculation for the average mass of the target element), Bohr straggling with the Chu/Yang correction and including multiple scattering is calculated, SRIM-2003 stopping powers are used, the scattering cross section for the $^{16}\text{O}(\alpha,\alpha)^{16}\text{O}$ is calculated with SigmaCalc, and Andersen electron screening (Andersen *et al.*, 1980) is calculated for the other elements.

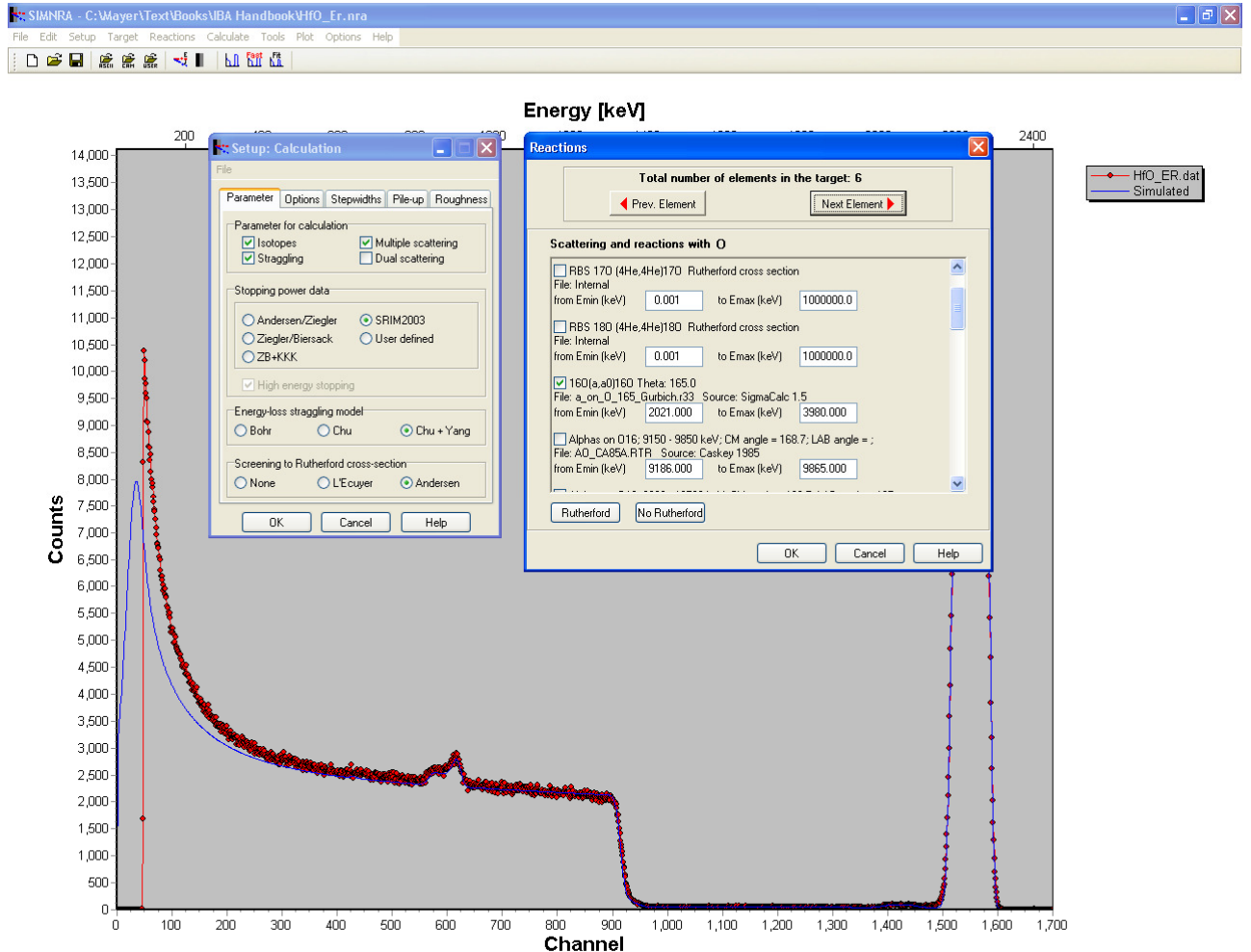


FIG. 14.13. Second step of a SIMNRA analysis: Configure simulation parameters.

Finally, the sample is defined: Layers are created, with any number of elements. The user inputs the thickness and concentration values, as well as roughness parameters if required. Then, a simulation is generated and compared to the data. The user can then iteratively refine the sample description until a good fit is reached or use a fitting routine to adjust the thickness and concentration of one layer at a time.

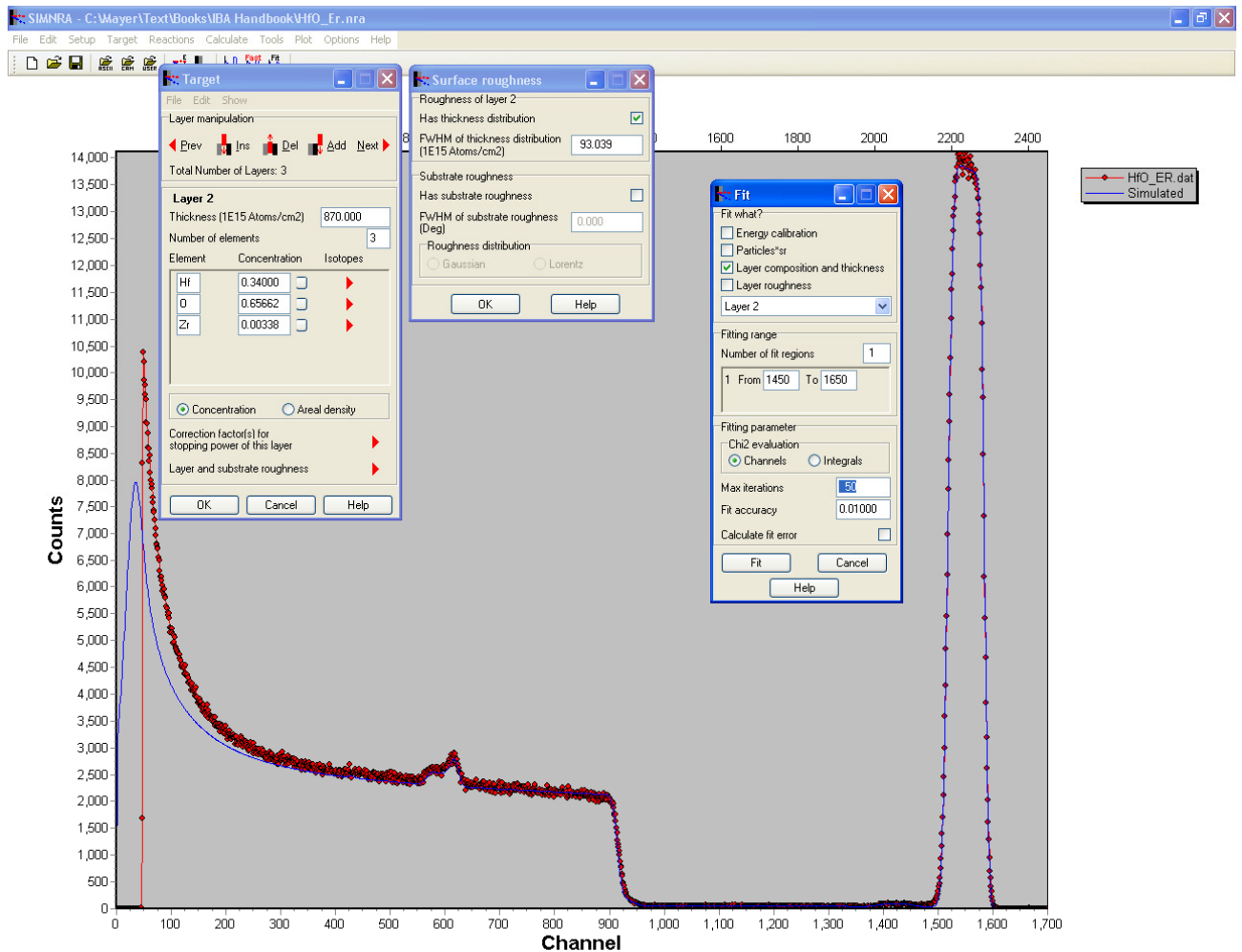


FIG. 14.14. Third step of a SIMNRA analysis: define the sample structure, perform the simulation. Here the final result is shown, after manual iteration until agreement between simulation and fit is achieved.

14.6.3 NDF

Development of NDF started in 1997. It can be run in Windows or DOS mode, in both Windows and UNIX.

We show in the NDF example (EXAMPLE 14.5) exactly the same spectrum as was used for the RUMP and SIMNRA examples. The main difference is that the final depth profile is reached without an initial guess being defined by the user.

EXAMPLE 14.5. NDF/DataFurnace.

In this example, sample E3 from the IAEA intercomparison exercise of IBA software (Barradas *et al.*, 2007b) is used. It is a hafnium oxide layer with impurities on a Si substrate, analysed by RBS with a 2.5 MeV $^4\text{He}^+$ beam. The first step after loading in the data is to define the experimental conditions. This is done by creating geometry files, one per each different set of experimental conditions used. In this case, only one measurement was made, so only one geometry file is required. The physics included in the calculation (the same as in RUMP and SIMRNA) is also input in the geometry file. Note that NDF does not make its own multiple scattering calculations; instead, it uses DEPTH in run time. The final step is to associate each spectrum with its corresponding geometry, in the main IBA DataFurnace window.

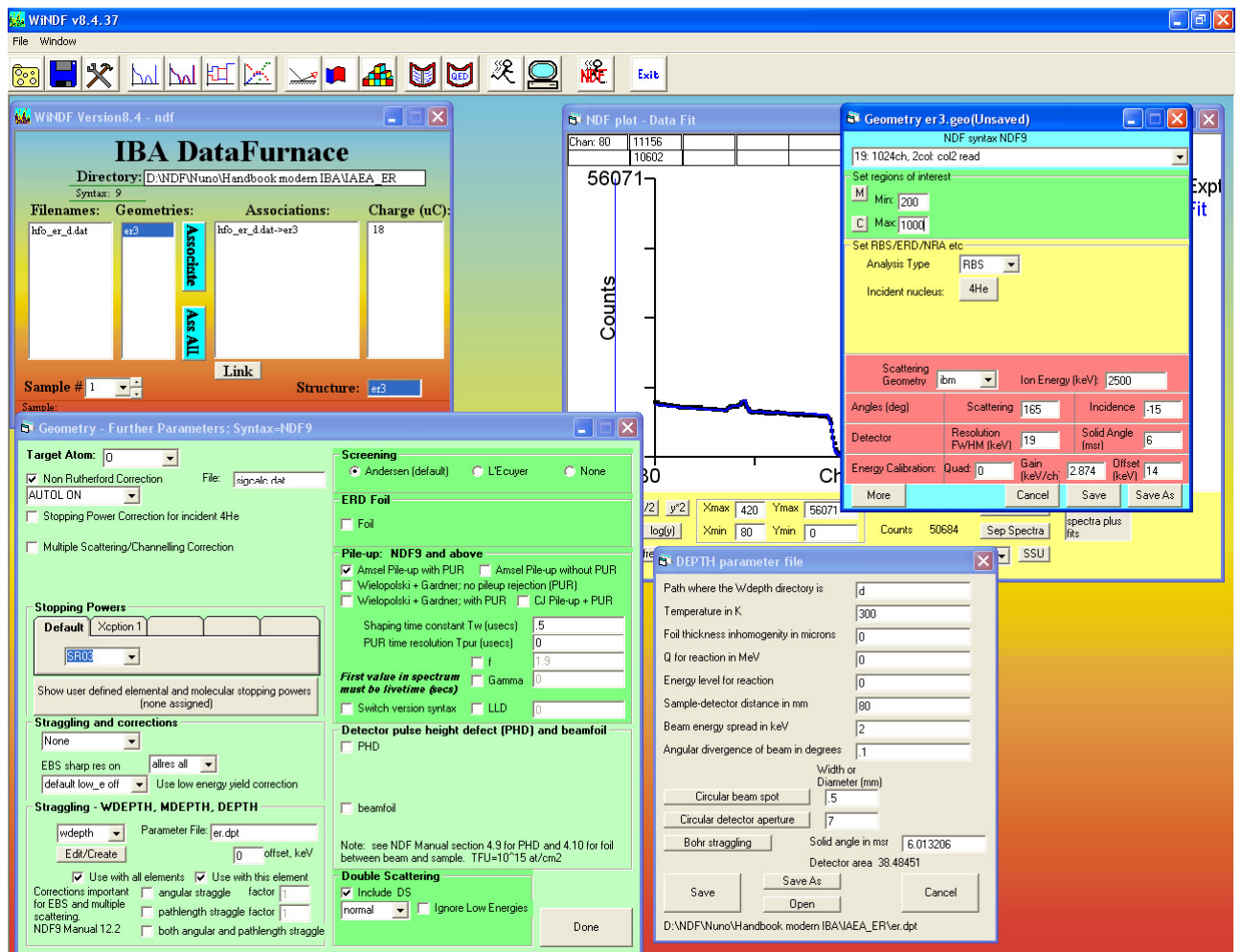


FIG. 14.15. First step of a NDF analysis: load the data and define the experimental conditions, configure simulation parameters.

The second step is to define which elements exist in the sample. This is done by creating a structure file with logical elements, which can be simple elements such as Si, molecules such as SiO₂ with a given density, or complex molecules with unknown stoichiometry to be determined in the fit. Restrictions on the depth and concentration ranges where each logical element can exist might also be given. If many completely different samples are to be analyzed in batch mode, one structure file is created for each sample. If many similar samples are to be analyzed, the same structure file is used for all of them.

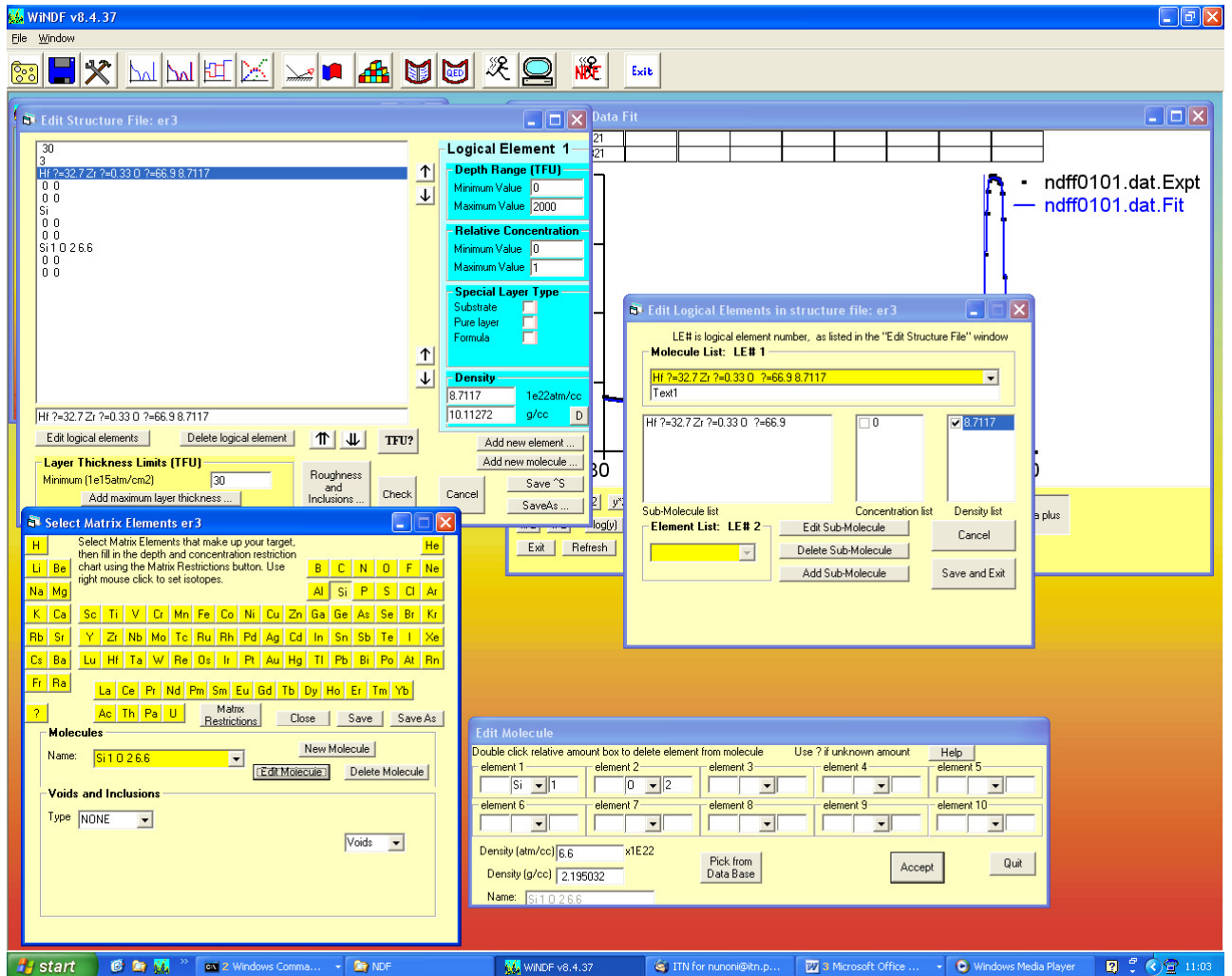


FIG. 14.16. Second step of a NDF analysis: define which elements or molecules are present in the sample.

The final step is to run an automated fit. In this case, the user does not have to define a layer structure; rather, this structure will be an output of the fit. The algorithm used, simulated annealing, tries to find the simplest structure consistent with the data. As the calculation is completely automated, the user must check the results, because it can find unwanted solutions. Alternatively, the user can also make an iterative analysis by defining a layer structure in the usual way. This can also be the initial guess for a local search on all parameters.

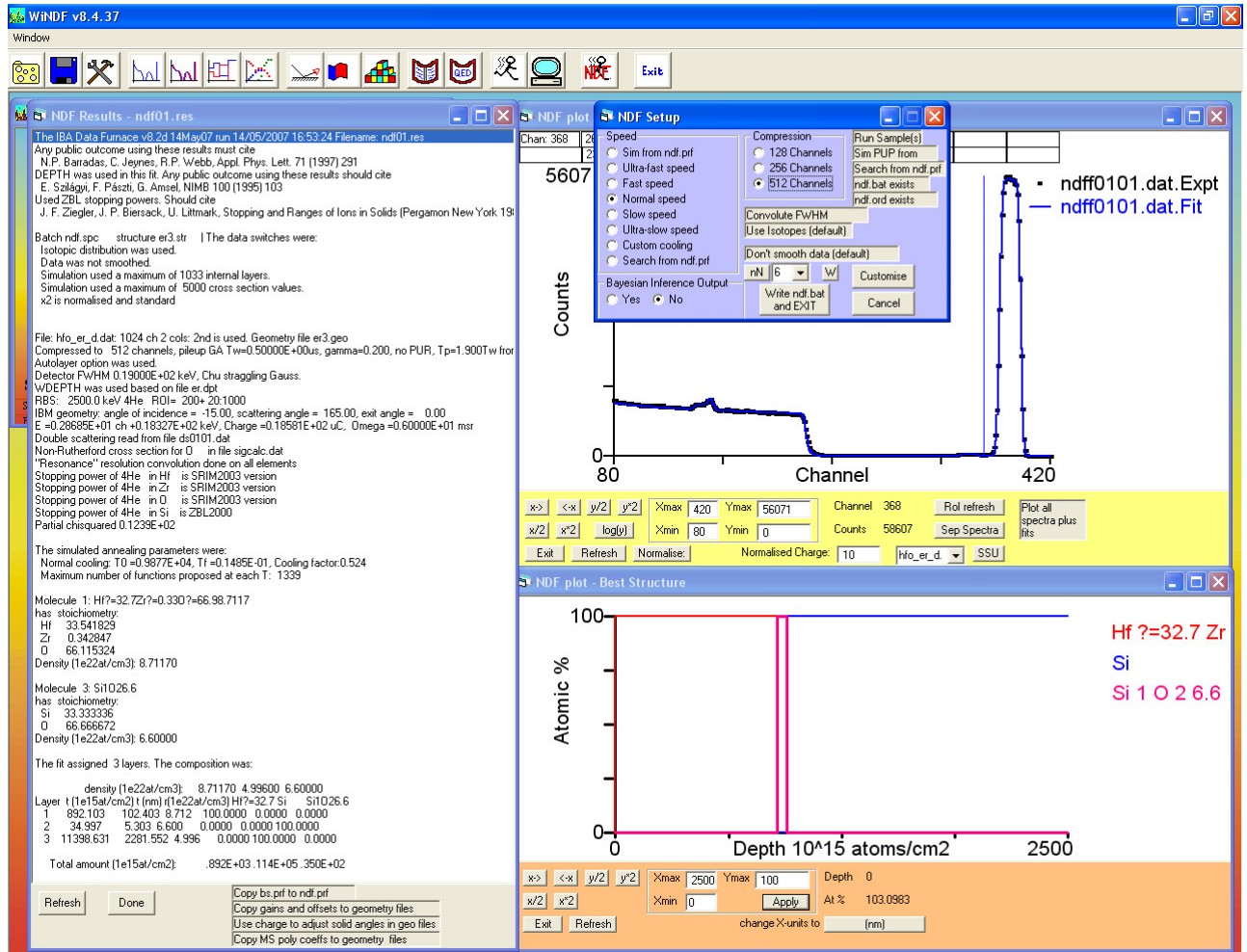


FIG. 14.17. Third step of a NDF analysis: run a fully automated fit, or, alternatively, perform an iterative analysis.

14.6.4 Issues

Both SIMNRA and NDF are being actively developed and supported. This means that users can rely on advice and help from the developers.

Both codes are strictly proprietary. The source code is restricted to the authors. This means that users cannot check whether the algorithms used are correct or not. Most users do not want to do this anyway, and the IAEA intercomparison of IBA software showed that the codes are essentially correct.

Both codes are only available commercially. Free test versions can be obtained, but to use the codes in research or industry, they must be purchased. This limits their availability. It also means that reliable first-generation codes will continue to be used in many cases. This is not a bad thing, as those codes are perfectly capable of handling many experimental data.

Some modules recently introduced in NDF (e.g., for PIXE and resonant NRA) are open source.

New-generation codes are more complex and difficult to use, which is normal given that they include many further options. This is another reason for the continuing use of first-generation codes in cases where the extra options are not necessary.

14.7 MONTE CARLO SIMULATION

The standard data analysis procedure described in the sections above uses deterministic algorithms. These can include physics through accurate or approximate implementations. All of the algorithms have limitations coming from two main sources: First, many phenomena are treated in a statistical way with disregard for the real particle–particle interactions that occur. Energy loss, energy-loss straggling, and multiple scattering are the three main phenomena in this category. In some cases, such as multiple scattering in grazing-angle conditions, the best models available (Amsel *et al.*, 2003) reach their limit of validity. Second, the details of the experimental setup are normally disregarded. For instance, calculations of geometrical straggling often disregard its influence on the scattering cross section (Szilágyi *et al.*, 1995; Rauhala *et al.*, 2006). Details of detection systems other than solid-state dispersive energy detectors, such as time-of-flight (TOF) systems, are not implemented in most standard codes.

In particular, standard codes have problems in the analysis of heavy-ion TOF-ERDA data, particularly at low energies where multiple scattering plays a very important role. Not only are signals broadened, but the actual yield is also not what would be expected from single scattering.

The alternative is to develop a Monte Carlo (MC) simulation of the individual particle–particle interactions. In practice, ion–electron interactions are not calculated, and tabulated stopping powers are used. Nevertheless, complex physical processes such as double and multiple scattering, as well as the full ion–detection system interaction, are taken into account in a natural way, without the approximations that standard codes involve.

Three MC codes for general-purpose analysis of ERDA data have been presented and applied to the analysis of different systems. MCERD and Corteo can also handle RBS data (Sajavaara *et al.*, 1998; Arstila *et al.*, 2001; Schiettekatte, 2008). The third code, FTHIE, is a fast Fortran version of TRIM for heavy-ion ERDA (Johnston *et al.*, 2000; Franich *et al.*, 2004). Other codes, such as RBSIM (Smulders and Boerma, 1987) and GEANT4 (Geil *et al.*, 2007), also exist.

EXAMPLE 14.6 of data analysis by MC illustrates very well the capabilities and limitations of MC simulations. All spectral features are reproduced, which allows the user to ascertain whether a given signal is relevant or not. In the example presented, it is possible to exclude the presence of O in the TaN layer with accuracy much better than what could be achieved by standard codes, which do not calculate plural and multiple scattering as accurately calculated as does MC. On the other hand, statistical oscillations

are observed in the calculation. They represent the accuracy of the MC calculation, which can be improved by using longer calculation times. Nevertheless, the calculation of backscattered ions, as well as of low energy signals, is inherently slower in MC simulations.

The main barrier to the general use of MC codes in routine data analysis, in addition to calculation times that are still longer than those required by standard codes, is that they are considered difficult to use. In some cases, no graphical user interface is available, and the user must edit input files and look at output files, which is very efficient for advanced users and rather difficult for everyone else. MC codes are not yet widely used except by the authors and their collaborators. This might change soon, as one of the MC codes, Corteo, now has a user-friendly windowed interface (Schiettekatte, 2008).

Nevertheless, the extraordinary quality of the simulations that can be achieved, particularly when plural and multiple scattering are important, means that MC simulations might be the basis for the next generation of codes, once issues with the user interface and computer speed are solved.

EXAMPLE 14.6. Monte Carlo.

We show in Fig. 14.18 a TOF measurement of a Si/SiO₂ (100 nm)/TaN (30 nm) sample measured with a 16 MeV ⁶³Cu beam, analyzed with MCERD. Recoils and backscattered Cu atoms were separated by the detection system.

The analysis, shown in Fig. 14.19, leads to the stoichiometries Si, 1.00 ± 0.02 ; O, 2.00 ± 0.02 ; and Ta, 0.47 ± 0.02 ; N, 0.53 ± 0.02 . The first comment is that the simulations include the statistical fluctuations expected from MC. The most important point is that extraordinarily good agreement with the data is obtained, even in the shape of the signal back edges and the low-energy backgrounds. This is essential, for instance, to rule out the presence of O in the TaN film. No standard code could achieve such results.

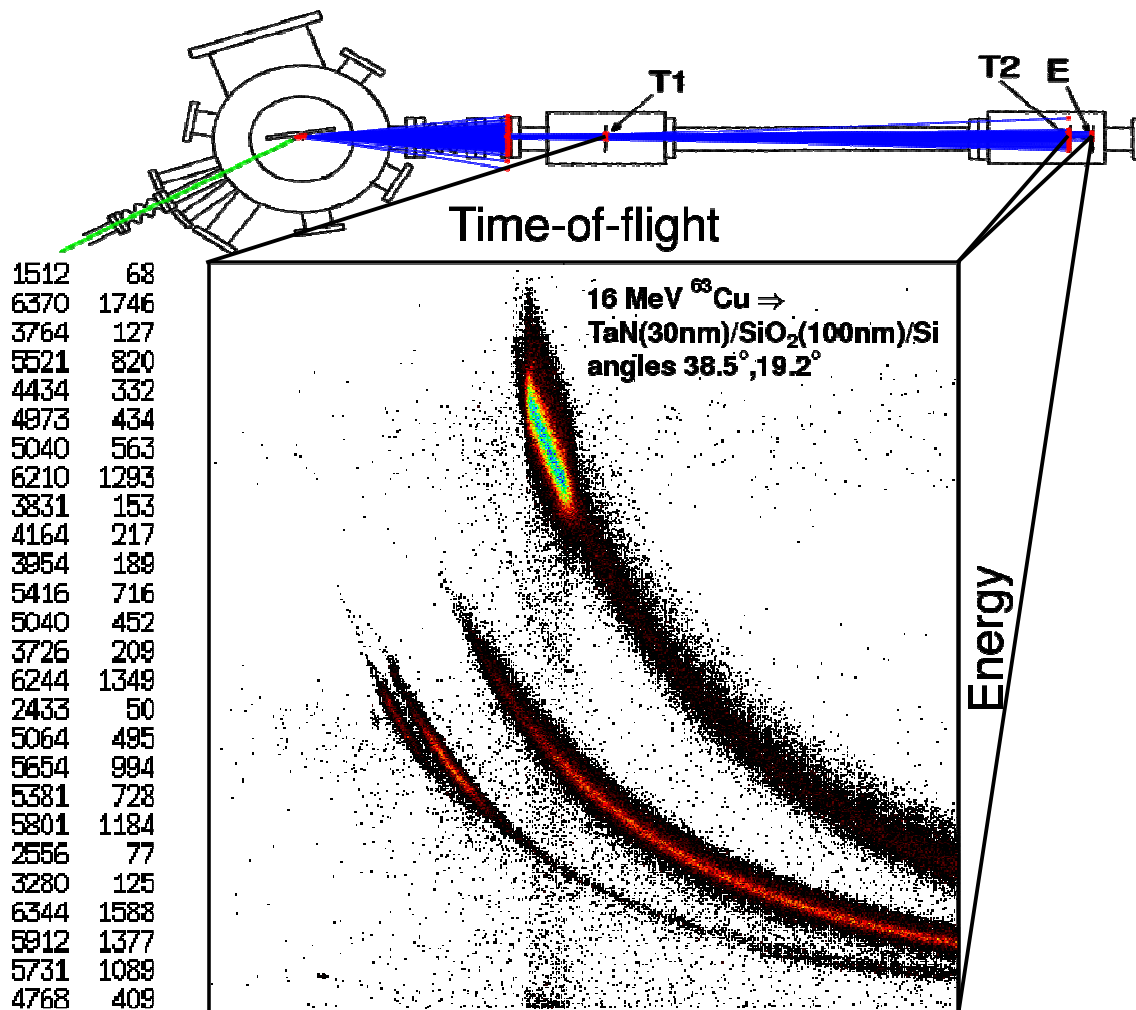


FIG. 14.18. Time-of-flight ERDA of a Si/SiO₂ (100 nm)/TaN (30 nm) sample measured with a 16 MeV ⁶³Cu beam.

The statistical fluctuation of the simulation is high for the Ta recoil signal. This is due to the low recoil cross section for this heavier target element. Also, the backscattering cross section is low, which means that the calculation of the Cu recoils can be orders of magnitude slower to reach the same statistical accuracy. These aspects are inherent to MC data analysis. Further improvements in the efficiency of the algorithms and in the computer speed can lead to faster simulation times, which are currently in the minute to hour range.

The Ta recoil signal is not as well simulated as the other elements, and a good simulation requires a slightly smaller layer thickness, which is not consistent with the data from the other elements. This is due to inaccuracies in the heavy-ion stopping-power databases, which are sparse and not as accurate as those for H and He, particularly at low velocities. This is a problem of the technique and not of the data analysis method, as all codes rely on the same stopping databases.

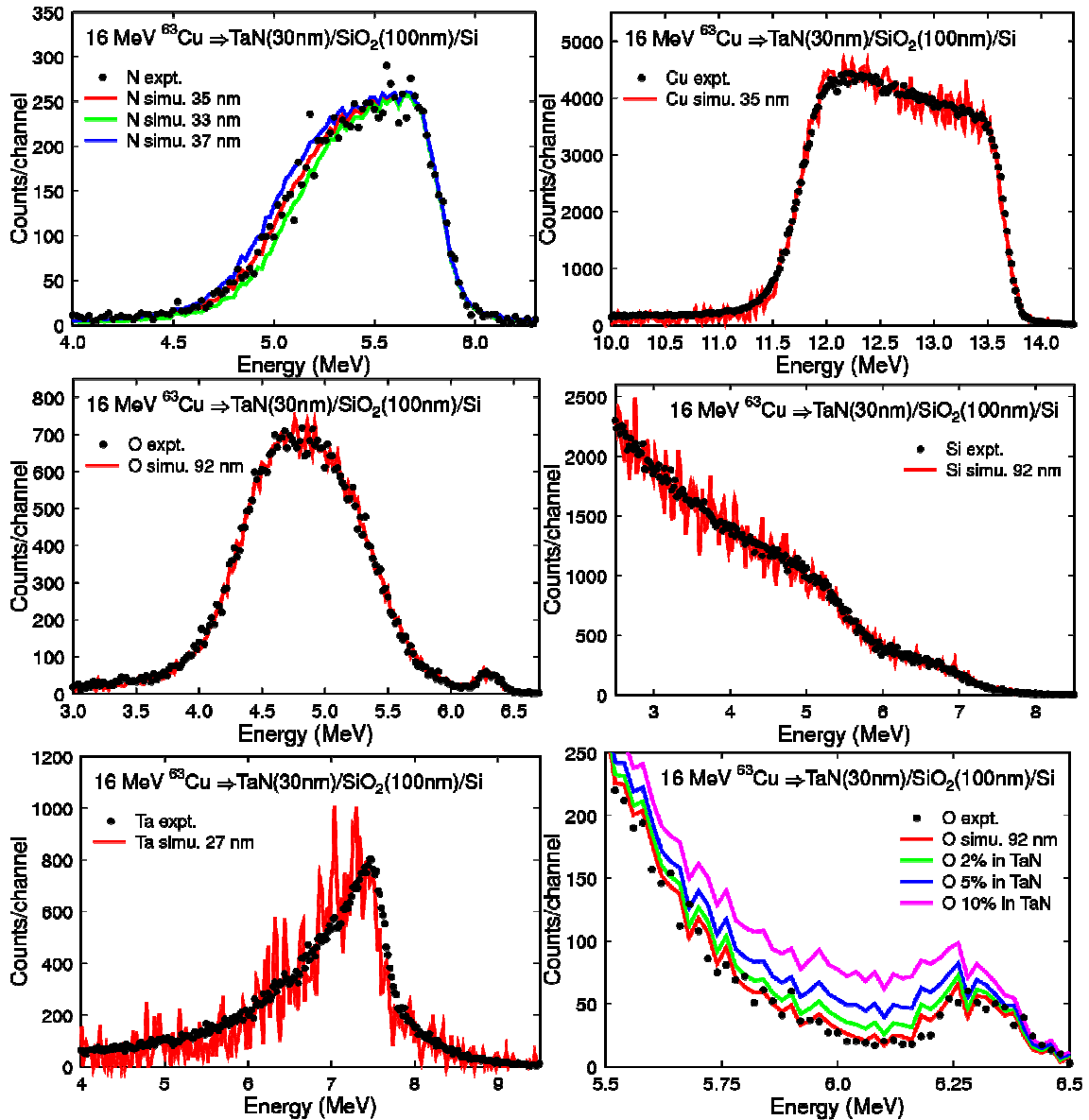


FIG. 14.19. MCERD analysis of TOF-ERDA of a Si/SiO₂ 100nm/TaN 30nm sample measured with a 16 MeV ^{63}Cu beam.

14.8 OTHER TECHNIQUES

In this section, only a brief mention of methods and codes used for data analysis of other techniques is made.

14.8.1 PIXE

Over the years, the PIXE community developed its own methods and codes for data analysis. The IAEA organized an intercomparison of PIXE codes (Blaauw *et al.*, 2002), but only very simple spectra were tested.

The best-known PIXE code is GUPIX (Maxwell *et al.*, 1995), which is used in many laboratories around the world. GUPIX is geared toward analyzing PIXE energy spectra

accurately, including those from multilayered targets. GUPIX is not designed to determine quantitative two-dimensional concentration maps from microbeam experiments.

AXIL (Van Espen *et al.*, 1977) and its free-of-charge version QXAS are also widely known.

The code GeoPIXE was developed more recently (Ryan *et al.*, 1990; Ryan, 2000). It has proved to be very powerful not only in the analysis of energy spectra, but also for quantitative two-dimensional analysis. It is also capable of analyzing multilayered targets, as well as three-dimensional inclusions by modeling PIXE yields from buried three-dimensional objects.

An alternative approach, AXSIA (Doyle *et al.*, 2006), uses multivariate spectral analysis. It has the advantage of being automated and nonbiased and can also, in principle, be used to combine different data sets, such as simultaneously collected micro-PIXE and micro-RBS data.

Already in the 1990s, PIXE was combined with RBS in the same code, through the so-called Q-factor method implemented in the user-friendly DAN32 package (Grime, 1996), which uses RUMP and GUPIX. A fit to the proton RBS spectrum collected simultaneously with the PIXE data is made. This fit is used to determine the actual collected charge, which is then used in the quantitative analysis of the PIXE data. This very useful improvement, however, does not ensure complete consistency between the analysis of the RBS and PIXE data, and it also does not fully take advantage of the combination of the depth sensitivity of RBS with the elemental and trace sensitivity of PIXE.

The open-source LibCPIXE library (Pascual-Izarra *et al.*, 2006b), based on the DATTPIXE code (Reis and Alves, 1992), also supports multilayered targets. It has been integrated in the general-purpose IBA data analysis code NDF (Jeynes *et al.*, 2003). Any number of PIXE spectra can be analyzed together with any number of RBS, ERDA, and NRA spectra, leading to one single depth profile consistent with all of the data. Similarly to GUPIX, this approach is geared toward spectra and not two-dimensional maps.

14.8.2 Resonant NRA, PIGE, NRP, MEIS, channeling, microscopies, and so on

This short section is dedicated to techniques and experimental conditions not yet covered in this chapter.

In several different techniques, the yield of a given nuclear reaction is determined as a function of the initial beam energy. Depth profile information can be extracted from the shape of the excitation curve obtained by scanning the beam energy.

The nuclear reaction is often a (elastic or inelastic) particle–particle reaction or a particle–gamma reaction. These techniques are often called resonant NRA and particle-induced gamma emission (PIGE), respectively. Different codes have been presented, such as ANALNRA by Johnston (1993), WinRNRA by Landry and Schaaf (2001), and ERYA by Mateus *et al.* (2005). NDF also implements this technique.

If a narrow resonance is used, normally isolated and background-free, together with a correspondingly small initial beam energy spread (each with a fwhm typically smaller than 0.5 keV), the term narrow resonance profiling (NRP) is used independently of the reaction type. In that case, it is necessary to take into detailed account the individual

energy-loss events to correctly calculate the excitation curves. The best-known code for that purpose is SPACES by Vickridge and Amsel (1990). It implements the stochastic theory of energy loss of Maurel *et al.* (1982), which allows the user to retrieve accurate high-resolution depth profiles. Codes that assume a Gaussian energy distribution of the beam will lead to inaccurate depth profiles, particularly near the surface. More recently, another code, FLATUS, was presented by Pezzi *et al.* (2005).

Medium-energy ion scattering (MEIS) could be seen as a particular case of RBS at low energies, but in fact, several important points must be considered, including special detector arrangements; the screened scattering cross section used; and also the fact that, for the high-resolution profiling that can be achieved with MEIS, stochastic energy loss must be considered (Pezzi *et al.*, 2007).

Specific methods have been developed for the analysis of channeling data. These include dedicated Monte Carlo codes (sometimes limited to specific systems), as well as different implementations of analytical theories. Monte Carlo codes such as FLUX by Smulders and Boerma (1987) and BISIC (Albertazzi *et al.*, 1996) are adequate for detailed studies of crystalline lattices, including lattice locations of impurities, defect configurations, and damage. Analytic codes such as DICADA (Gärtner, 2005) and RBX (Kótai, 1994) are less accurate but possibly easier to use in the study of defect profiles. RBX is the only standard all-purpose data analysis code that includes channeling.

Different ion-based microscopies have been developed. These range from the two-dimensional maps collected with PIXE to techniques such as scanning transmission ion microscopy (STIM). They all have dedicated methods of data analysis. Particular applications often require the development of specific methods. These are beyond the scope of this chapter.

Artificial neural networks have been developed by Barradas, Vieira, and co-workers for the unattended automatic analysis of IBA data and applied to a variety of systems, from the very simple to the very complex (Barradas and Vieira, 2000; Nené *et al.*, 2006). This approach can be of practical importance only when large numbers of similar spectra are collected, as in quality-control applications, for example, or in the analysis of data collected in real-time RBS experiments, where hundreds or thousands of spectra are collected within a few days (Demeulemeester *et al.* 2008).

Finally, many codes and data analysis codes have been developed over the years for very specific applications and experimental conditions. We refer the reader to the review by Rauhala *et al.* (2006), and the references therein, where several of these codes are discussed.

14.9 THE IBA DATA FORMAT IDF

IBA data analysis codes such as RUMP, SIMNRA, NDF, and others all use and implement various formats to store the data and to describe the experimental conditions and simulation or fit parameters. RUMP reads and writes both specific ASCII and binary formats. SIMNRA reads and writes a specific ASCII based format. NDF is user-driven and reads over 30 different ASCII and binary formats, but it writes specific files.

This is a strong barrier against interchange of data between people from different laboratories, or that use different set-ups to measure their data, different computers to store their data, and different data analysis programs to analyse their data.

A new IBA data format, called IDF, that aspires to support all forms of IBA data in a well defined simple format permitting easy exchange between sites and analysis programs was presented in the 19th IBA International Conference, and will be implemented in NDF, RUMP and SIMNRA by the end of 2009.

The main characteristics of the IDF are: 1) It can be read and understood by human inspection of the file, i.e. it is ASCII. This makes it portable amongst all hardware platforms and operating systems, and it is self-explanatory 2) It is flexible enough to cater to all IBA data needs, so a file entry can correspond to one given sample, or to a group of similar samples, or to one experimental run, or it may contain simulations only, or anything else that the user may need. 3) It is easily extendable; most commonly used features are already included, but special needs are easy to incorporate by any user.

The IDF was implemented as an extensible mark-up language (XML) format. XML was developed by the World Wide Web Consortium (W3C) to structure, store, and transport data. It was chosen as the IDF development platform because it is a recognised standard that fulfills the specifications defined.

The definition of the IDF, including full documentation and examples is given in <http://idf.schemas.itn.pt>.

ACKNOWLEDGEMENTS

We thank Mike Thompson, Matej Mayer, and Kai Arstila for providing the figures for the RUMP, SIMNRA, and MCERD examples, as well as all those who commented on early drafts.

Table 14.2. General information about analysis programs.

Analysis program	Technical contact	Current status	Distribution mode	Status of source code	Operating system(s)
DEPTH	Edit Szilágyi KFKI Research Institute for Particle and Nuclear Physics Budapest, Hungary szilagyi@rmki.kfki.hu ; www.kfki.hu/~ionhp/	Active development	No charge; downloadable from Web site	Restricted to author/not available	DOS and Windows
GISA	Eero Rauhala University of Helsinki, Helsinki, Finland and Jaakko Saarilahti, Technical Research Center of Finland Eero.rauhala@helsinki.fi ; Jaakko.Saarilahti@vtt.fi	In use	No charge; write to author for copy	Restricted to author/not available	DOS (or emulators)
MCERD	Kai Arstila IMEC, Leuven, Belgium kai.arstila@iki.fi	Active development	No charge; write to author for copy	Source code available	Linux (Windows)
NDF (DataFurnace)	Nuno Barradas Technological and Nuclear Institute Sacavém, Portugal nunoni@itn.pt ; www.ee.surrey.ac.uk/Research/SCRIBA/ndf/	Active development	Commercially available through Univ. of Surrey; evaluation copies available upon request	Restricted to author/not available; some modules open source	Windows, DOS, UNIX
RBX	Endre Kótai KFKI Research Institute for Particle and Nuclear Physics Budapest, Hungary kotai@rmki.kfki.hu	Active development	No charge; write to author for copy	Restricted to author/not available	Windows
RUMP	Mike Thompson Dept. of Materials Science, Cornell University Ithaca, NY USA motl@cornell.edu ; www.genplot.com	Active development	Commercially available through Computer Graphics Service; evaluation copies available from Web site	Source code available	Windows, Linux, UNIX, OS2
SIMNRA	Matej Mayer MPI for Plasma Physics Garching, Germany Matej.Mayer@ipp.mpg.de ; www.rzg.mpg.de/~mam/	Active development	Commercially available through MPI for Plasma Physics; evaluation copies available from Web site	Restricted to author/not available	Windows

Table 14.3. User interface properties of the analysis programs.

Analysis program	Nature of the primary interface	Primary simulation modes	Graphical output
DEPTH	Interactive or batch	Manual iteration	N/A
GISA	Interactive	Manual iteration; automated parameter search	Screen only
MCERD	Batch	Manual iteration	N/A
NDF (DataFurnace)	Batch directed or interactive	Fully automated search; manual iteration	Publication quality
RBX	Interactive	Manual iteration	Draft quality
RUMP	Interactive	Manual iteration; automated parameter search	Publication quality
SIMNRA	Interactive	Manual iteration; automated parameter search	Draft quality

Table 14.4. Fundamental databases used by analysis programs.

Analysis program	Stopping powers	Cross sections
DEPTH	ZBL'95	User-defined from file
GISA	TRIM1991 or Ziegler and Chu; user-defined correction per layer	User-defined from file
MCERD NDF (DataFurnace)	ZBL'96 or user-defined ZBL'95, SRIM, KKKNS (Si), MSTAR Ability to load experimental values; user-defined correction per ion/element	Rutherford, user-defined from file to be included User-defined from file
RBX	ZBL'95 with channeling correction possible; user-defined correction per layer	Internal (modifiable) library of cross sections; external cross-section Library Editor (import Sigabase R33; user-defined)
RUMP	ZBL'92, SRIM, KKKNS User-defined compounds and databases; user-defined correction per layer or per element	IBANDL, SigmaCalc; user-defined
SIMNRA	SRIM-1997, SRIM, or KKKNS User-defined correction per layer and ion	IBANDL, SigmaCalc; user-defined

Table 14.5. Fundamental physics handled in the simulations.

Analysis program	Isotope calculation	Screening calculation	Straggling models	Plural scattering	Multiple scattering	Geometric straggling	Channeling
DEPTH	Single isotope	Yes	Bohr, Chu, Yang, Tschalär	None	Yes, Pearson VII distribution	Yes	No
GISA	Natural abundance and/or specific isotopes	Energy/angle; external tables by users	Bohr + Lindhard/Scharff	None	None	No	No
MCERD	Natural abundance and/or specific isotopes	No	Bohr, Chu, Yang	Full MC calculation	Full MC calculation	Yes	No
NDF (DataFurnace)	Natural abundance and/or specific isotopes	Energy/angle; Andersen and L'Ecuyer	Bohr, Chu, Yang, Tschalär	Dual scattering approx. (run-time option)	Yes, Gaussian approximation from DEPTH calculation	Yes, from DEPTH calculation	No
RBX	Natural abundance and/or specific isotopes	Yes	Bohr, Chu, Yang, Tschalär	None	Yes (same model as DEPTH)	Yes	Defect calculation; simulation of channeled spectra
RUMP	Natural abundance and/or specific isotopes	Energy only; L'Ecuyer	Bohr	None	None	No	No
SIMNRA	Natural abundance and/or specific isotopes	Energy/angle; Andersen and L'Ecuyer	Bohr, Chu, Yang, Tschalär	Dual scattering approx. (run-time option)	Yes (DEPTH model approximated as Gaussian)	Yes	No

Table 14.6. Experimental conditions and simulation capabilities.

Analysis program	Incident ions	Analytical technique(s)	Scattering geometry(ies)	Pileup correction	Detection system(s)	Stopper foils	Energy calibration
DEPTH	All	RBS, ERDA, NRA	IBM, Cornell	No	Energy-dispersive (magnetic spectrograph coming)	Simulated; including inhomogeneities	Linear
GISA	All	RBS	IBM	No	Energy-dispersive	N/A	Quadratic
MCERD	All	ERDA, RBS	IBM	No	Energy-dispersive; TOF; different layers in detector for gas detectors, for example	Simulated; equivalent treatment to sample	Linear
NDF (DataFurnace)	All	RBS, ERDA, nonresonant NRA, PIXE, resonant NRA (PIGE, NRP)	IBM, Cornell, General	Yes	Energy-dispersive	Simulated; equivalent treatment to sample	Quadratic; varying by ion species
RBX	All	RBS, ERDA, nonresonant NRA	IBM, Cornell	Yes	Energy-dispersive	Simulated; homogeneous foils only	Linear
RUMP	All	RBS, ERDA	Cornell, IBM, General	Yes	Energy-dispersive, partial TOF	Simulated or from user calibration	Linear
SIMNRA	All	RBS, ERDA, nonresonant NRA	IBM, Cornell, General	Yes	Energy-dispersive, TOF, electrostatic, thin solid-state detectors with transmission of particles	Simulated; equivalent treatment to sample	Quadratic; varying by ion species

Table 14.7. Fitting capabilities DEPTH and RBX have no fitting capabilities).

Analysis program	Starting conditions	Optimization method	Error estimation	Statistics used	Searchable experimental parameters	Auto-refinement of layers	Limitations
GISA	Reasonable guess	χ^2 minimization	None returned		None	No	One layer at a time
NDF (DataFurnace)	Elements only; guess can be used but not required	Simulated annealing plus grid search	Bayesian inference with Markov chain Monte Carlo integration (time-intensive)	Poisson	E_0 , E_{cal} , charge, θ , Φ , φ	Yes	All parameters variable, user controls which ones change
RUMP	Reasonable guess	Marquart search	Curvature of χ^2 matrix; full correlation of error sensitivities (intrinsic to search method)	Poisson	E_0 , E_{cal} , charge, current, θ , Φ , φ	No	No internal limit, practical of 30 parameters at a time
SIMNRA	Reasonable guess	Simplex search	Additional search to determine curvature near best fit (comparable to fit time)	Poisson	E_{cal} , charge	No	One layer at a time, all characteristics

Table 14.8. Sample definition and complexity handled.

Analysis program	Sample description	Continuous profiles	Slab limitations/elements	Substrate roughness	Layer roughness
DEPTH	Layer definition	Slabs only	None	No	No
GISA	Layer definition or profile function	Maps continuous profiles onto slab structure	10 layers; 10 elements; user can define so layer*element is constant	No	No
MCERD					
NDF (DataFurnace)	Layer definition; use of profile function	Effective error function interdiffusion profiles between layers	250 layers in description; up to 92 constituents	Yes; approximated as energy broadening	Yes; approximated as energy broadening
RBX	Layer definition	User-defined functions (Gauss, error functions, etc.); channeling defect distributions	None	No	No
RUMP	Layer definition with equation overlays	Gaussian implants, error function diffusion, Pearson IV profiles, one-sided and two-sided diffusion	None	No	Yes; single- or dual-sided, all interfaces possible
SIMNRA	Layer definition; use of profile function	Slabs only	100 layers in description; 40 elements per layer	Yes; Lorentzian or Gaussian angular distribution	Yes; all interfaces possible

Table 14.9. Effects of some phenomena on data analysis.

phenomenon	Ion	Energy	Scattering angle	Target element	Effect on spectrum	Error	Effect on analysis
cross section							false quantitative analysis
electron screening	All	All	<15°	All	Decreased yield	Unknown (large)	
	All	>150 keV/Z ₁	>15°	Heavy		1%	
	All	>500 keV/Z ₁	>90°	Heavy		≥0.2%	
nuclear effects	p	≥100 keV	All	Light (medium heavy)	Increased or decreased yield	Depends on reaction (can be large)	
	α	≥2.0 MeV	All	Light			
stopping power							false quantitative and depth analysis
general uncertainties*	p			All	Increased or decreased yields and widths	4.2% average (>10% for 13% of target atoms)	
	α			All		4.1% average (>10% for 11% of target atoms)	
	α			Si		≤2%	
	Li			All		5.1% average (>10% for 17% of target atoms)	
	Heavier ions			All		6.1% average (>10% for 18% of target atoms)	
Bragg rule violations	All			Light compounds (insulators)	Increased or decreased yields and widths	≤10°15%	
physical state effects	All			Light solids versus liquid or gaseous	Increased or decreased yields and widths	≤5°10%	
energy spread, multiple scattering	Heavy		Grazing-angle geometry		Increased or decreased edge and peak broadness	Large	false interdiffusion, mixing, depth profile, and roughness analysis
	p		Normal incidence			Small	
	All		All			Depends on details (can be small or large)	
surface roughness	All			All	Increased edge and peak broadness	Depends on details (can be small or large)	false analysis of intermixing and interdiffusion
channeling	All		Incidentally aligned geometry		Decreased yields	Depends on details (can be small or large)	false quantitative and depth analysis
pulse pileup	All			Heavy (all)	Increased or decreased yields, background	≤2–5% for count rates below ~5 kHz	false quantitative analysis, reduced sensitivity
low-energy background	All	Low (all)	Grazing geometry (all)	Heavy (all)	Increased background	Depends on the details; can be dominant at low energies; small in most analyses	false quantitative analysis, reduced sensitivity

*The errors quoted refer to SRIM-2003.

SOFTWARE WEB SITES

This list of web sites relevant for IBA software and data analysis is by no means complete. Several of the codes mentioned in this chapter have no dedicated Web site.

Corteo	http://www.lps.umontreal.ca/~schiette/index.php?n=Recherche.Corteo Monte Carlo (MC) simulation program for ion beam analysis spectra
DEPTH	http://www.kfki.hu/~ionhp/doc/prog/wdepth.htm Windows-based program for calculating the energy and depth resolution of ion beam analysis methods such as Rutherford backscattering spectrometry (RBS) and elastic recoil detection analysis (ERDA)
FLUX	http://members.home.nl/p.j.m.smulders/FLUX/HTML/ Program for simulating the trajectories of high-energy ions in single crystals in channeling, or near-channeling, directions
GeoPIXE	http://www.nmp.csiro.au/GeoPIXE.html Software package that performs real-time particle-induced X-ray emission (PIXE)/synchrotron X-ray fluorescence (SXRF) spectral deconvolution using dynamic analysis
GUPIX/ GUPIXWIN	http://pixe.physics.uoguelph.ca/gupix/main/ Software package for fitting particle-induced X-ray emission (PIXE) spectra from thin, thick, intermediate, and layered specimens
IBANDL	http://www-nds.iaea.org/ibandl/ Library of experimental data on nuclear cross sections and excitation functions relevant to ion beam analysis (IBA); resulted from the merger SigmaBase and NRABASE
IBIS	http://www.kfki.hu/~ionhp/ Collection of resources for the ion beam community (called the Ion Beam Information System) that includes links to several programs and other useful sites, as well as an archive of documents
IDF	http://idf.schemas.itn.pt Definition of the IBA data format IDF, including documentation and examples
LibCPIXE	http://sourceforge.net/projects/cpixe Library for the simulation of particle-induced X-ray emission (PIXE) spectra
MSTAR	http://www.exphys.uni-linz.ac.at/stopping/ Collection of data on stopping powers of light and heavy ions
NDF	http://www.itn.pt/facilities/lfi/ndf/uk_lfi_ndf.htm General-purpose code for the analysis of Rutherford backscattering

	spectrometry (RBS), elastic recoil detection analysis (ERDA), particle-induced X-ray emission (PIXE), non-resonant nuclear reaction analysis (NRA), and neutron depth profiling (NDP) data for any ion, any target, any geometry, and any number of spectra
DataFurnace	http://www.ee.surrey.ac.uk/SCRIBA/ndf/ Fitting code (not a simulator) that extracts elemental depth profiles from Rutherford backscattering and related ion beam analysis spectra
QXAS	http://www.iaea.org/OurWork/ST/NA/NAAL/pci/ins/xrf/pciXRFdown.php DOS-based software package (called Quantitative X-ray Analysis System) for quantitative X-ray fluorescence analysis
RUMP	http://www.genplot.com Graphical data analysis and plotting package that provides comprehensive analysis and simulation of Rutherford backscattering spectrometry (RBS) and elastic recoil detection (ERD) spectra
SigmaCalc	http://www-nds.iaea.org/sigmacalc/ Service providing evaluated (recommended) differential cross sections for ion beam analysis
SIMNRA	http://www.rzg.mpg.de/~mam/ Windows-based program for the simulation of backscattering spectra for ion beam analysis with megaelectronvolt ions, mainly intended for non-Rutherford backscattering, nuclear reaction analysis (NRA), and elastic recoil detection analysis (ERDA)
SRIM	http://www.srim.org Group of programs that calculate the stopping and range of ions in matter using a quantum mechanical treatment of ion-atom collisions

REFERENCES

- Albertazzi, E., Bianconi, M., Lulli, G., Nipoti, R., and Cantiano, M. (1996), *Nucl. Instrum. Methods* **B118**, 128.
- Alkemade, P.F.A., Habraken, F.H.P.M., and van der Weg, W.F. (1990), *Nucl. Instrum. Methods* **B45**, 139.
- Amsel, G. (1996), *Nucl. Instrum. Methods* **B118**, 52.
- Amsel, G., Battistig, G., and L'Hoir, A. (2003), *Nucl. Instrum. Methods* **B201**, 325.
- Andersen, H.H., Besenbacher, F., Loftager, P., and Möller, W. (1980), *Phys. Rev.* **A21**, 1891.
- Arstila, K., Sajavaara, T., and Keinonen, J. (2001), *Nucl. Instrum. Methods* **B174**, 163.
- Barradas, N.P., Jeynes, C., Jenkin, M., and Marriott, P.K. (1999), *Thin Solid Films* **343–344**, 31.
- Barradas, N.P., and Vieira, A. (2000), *Phys. Rev.* **E62**, 5818
- Barradas, N.P. (2004), *Nucl. Instrum. Methods* **B225**, 318.
- Barradas, N.P., Alves, E., Jeynes, C., and Tosaki, M. (2006), *Nucl. Instrum. Methods* **B247**, 381.
- Barradas, N.P. (2007), *Nucl. Instrum. Methods* **B261**, 418.
- Barradas, N.P., Pezzi, R.P., and Baumvol, I.J.R. (2007a), *Nucl. Instrum. Methods* **B261**, 422.
- Barradas, N.P., Arstila, K., Battistig, G., Bianconi, M., Dytlewski, N., Jeynes, C., Kótai, E., Lulli, G., Mayer, M., Rauhala, E., Szilágyi, E., and Thompson, M. (2007b), *Nucl. Instrum. Methods* **B262**, 281.
- Bichsel, H (2006), *Nucl. Instrum. Methods* **A562**, 154.
- Blaauw, M., Campbell, J.L., Fazinić, S., Jakšić, M., Orlic, I., and Van Espen, P. (2002), *Nucl. Instrum. Methods* **B189**, 113.
- Bohr, N. (1948), *Mat. Fys. Medd. K. Dan. Vidensk. Selsk.* **18** (8).
- Børgesen, P., Behrisch, R., and Scherzer, B.M.U. (1982), *Appl. Phys.* **A27**, 183.
- Boudreault, G., Jeynes, C., Wendler, E., Nejm, A., Webb, R.P., and Wätjen, U. (2002), *Surf. Interface Anal.* **33**, 478.
- Butler, J.W. (1990), *Nucl. Instrum. Methods* **B45**, 160.
- Chu, W.K. (1976), *Phys. Rev.* **A13**, 2057.
- Demeulemeester, J., Smeets, D., Van Bockstael, C., Detavernier, C, Comrie, C.M., Barradas, N.P., Vieira, A., and Vantomme, A. (2008), *Appl. Phys. Lett.* **93**, 261912.
- Doolittle, L.R. (1985), *Nucl. Instrum. Methods* **B9**, 344.

- Doyle, B.L., Provencio, P.P., Kotula, P.G., Antolak, A.J., Ryan, C.G., Campbell, J.L., Barrett, K. (2006), *Nucl. Instrum. Methods* **B249**, 828.
- Eckstein, W., and Mayer, M. (1999), *Nucl. Instrum. Methods* **B153**, 337.
- Edelmann, E., Arstila, K., and Keinonen, J. (2005), *Nucl. Instrum. Methods* **B228**, 364.
- Franich, R.D., Johnston, P.N., and Bubb, I.F. (2004), *Nucl. Instrum. Methods* **B219–220**, 87.
- Gardner, R.P., and Wielopolski, L. (1977), *Nucl. Instrum. Methods* **140**, 289.
- Gärtner, K. (2005), *Nucl. Instrum. Methods* **B227**, 522.
- Geil, R.D., Mendenhall, M., Weller, R.A., and Rogers, B.R. (2007), *Nucl. Instrum. Methods* **B256**, 631.
- Grime, G.W. (1996), *Nucl. Instrum. Methods* **B109–110**, 170.
- Gurbich, A.F. (1997), *Nucl. Instrum. Methods* **B129**, 311.
- Gurbich, A.F. (1998), *Nucl. Instrum. Methods* **B145**, 578.
- Gurbich, A.F. (2005), in *Nuclear Data for Science and Technology* (Haight, R.C., Chadwick, M.B., Kawano, T., and Talou, P., eds.), AIP Conference Proceedings, American Institute of Physics, New York, vol. 769, p. 1670.
- Harjuoja, J., Väyrynen, S., Putkonen, M., Niinistö, L., and Rauhala, E. (2007), *Appl. Surf. Sci.* **253**, 5228.
- Jeynes, C., Barradas, N.P., Rafla-Yuan, H., Hichwa, B.P., and Close, R. (2000a), *Surf. Interface Analysis* **30**, 237.
- Jeynes, C., Barradas, N.P., Wilde, J.R., and Greer, A.L. (2000b), *Nucl. Instrum. Methods* **B161–163**, 287.
- Jeynes, C., Barradas, N., and Webb, R. (2000c), *The University of Surrey Ion Beam Centre IBA DataFurnace Users Guide*, University of Surrey Ion Beam Centre, Guildford, England, <http://www.ee.surrey.ac.uk/IBC/ndf/windfmanual70.pdf>.
- Jeynes, C., Barradas, N.P., Marriott, P.K., Boudreault, G., Jenkin, M., Wendler, E., and Webb, R.P. (2003), *J. Phys. D: Appl. Phys.* **36**, R97.
- Jeynes, C., Peng, N., Barradas, N.P., and Gwilliam, R.M. (2006), *Nucl. Instrum. Methods*. **B249**, 482.
- Johnston, P.N. (1993), *Nucl. Instrum. Methods* **B79**, 506.
- Johnston, P.N., Franich, R.D., Bubb, I.F., El Bouanani, M., Cohen, D.D., Dytlewski, N., and Siegele, R. (2000), *Nucl. Instrum. Methods* **B161–163**, 314.
- Kirkpatrick, S., Gelatt, C.D., and Vecchi, M.P. (1983), *Science* **220**, 671.
- Kótai, E. (1994), *Nucl. Instrum. Methods* **B85**, 588.
- Landry, F., and Schaaf, P. (2001), *Nucl. Instrum. Methods* **B179**, 262.

- L'Ecuyer, J., Davies, J.A., and Matsunami, N. (1979), *Nucl. Instrum. Methods* **160**, 337.
- Mateus, R., Jesus, A.P., and Ribeiro, J.P. (2005), *Nucl. Instrum. Methods* **B229**, 302.
- Maurel, B., Amsel, G., and Nadai, J.P. (1982), *Nucl. Instrum. Methods* **197**, 1.
- Maxwell, J.A., Teesdale, W.J., and Campbell, J.L. (1995), *Nucl. Instrum. Methods* **B95**, 407.
- Mayer, M. (1997), *SIMNRA User's Guide*, Technical Report IPP9/113, Max-Planck-Institut für Plasmaphysik, Garching, Germany.
- Mayer, M. (2002), *Nucl. Instrum. Methods* **B194**, 177.
- Mayer, M., Fischer, R., Lindig, S., von Toussaint, U., Stark, R.W., and Dose, V. (2005), *Nucl. Instrum. Methods* **B228**, 349.
- Mayer, M. (2007), *SIMNRA User's Guide*, Max-Planck-Institut für Plasmaphysik, Garching, Germany, <http://www.rzg.mpg.de/%7Emam/>.
- Mayer, M. (2008), *Nucl. Instrum. Methods* **B266**, 1852.
- Molodtsov, S., Gurbich, A.F., and Jeynes, C. (2009), *J. Phys. D: Appl. Phys.* **41**, Article Number 205303.
- Molodtsov, S., and Gurbich, A.F. (2009), *Nucl. Instrum. Methods* **B**, [doi:10.1016/j.nimb.2009.08.008](https://doi.org/10.1016/j.nimb.2009.08.008).
- Nené, N.R., Vieira, A., and Barradas, N.P. (2006), *Nucl. Instrum. Methods* **B246**, 471
- Neumaier, P., Dollinger, G., Bergmaier, A., Genchev, I., Görgens, L., Fischer, R., Ronning, C., and Hofsäss, H. (2001), *Nucl. Instrum. Methods* **B183**, 48.
- Padayachee, J., Meyer, K.A., and Prozesky, V.M. (2001), *Nucl. Instrum. Methods* **B181**, 122.
- Pascual-Izarra, C., Reis, M.A., and Barradas, N.P. (2006a), *Nucl. Instrum. Methods* **B249**, 780.
- Pascual-Izarra, C., Barradas N.P., and Reis, M.A. (2006b), *Nucl. Instrum. Methods* **B249**, 820.
- Paul, H., and Schinner, A. (2001), *Nucl. Instrum. Methods* **B179**, 299.
- Paul, H., and Schinner, A. (2002), *Nucl. Instrum. Methods* **B195**, 166
- Pezzi, R.P., Wallace, R.M., Copel, M., and Baumvol, I.J.R. (2005), *AIP Conf. Proc.* **788**, 571.
- Pezzi, R.P., Grande, P.L., Copel, M., Schiwietz, G., Krug, C., and Baumvol, I.J.R. (2007), *Surf. Sci.* **601**, 5559.
- Rauhala, E. (1984), *J. Appl. Phys.* **56**, 3324.
- Rauhala, E. (1987), *J. Appl. Phys.* **62**, 2140.

- Rauhala, E., Barradas, N.P., Fazinic, S., Mayer, M., Szilágyi, E., and Thompson, M. (2006), *Nucl. Instrum. Methods* **B244**, 436.
- Reis, M.A., and Alves, L.C. (1992), *Nucl. Instrum. Methods* **B68**, 300.
- Ryan, C.G., Cousens, D.R., Sie, S.H., Griffin, W.L., and Suter, G.G. (1990), *Nucl. Instrum. Methods* **B47**, 271.
- Ryan, C.G. (2000), *Int. J. Imaging Syst. Technol.* **11**, 219.
- Saarilahti J., and Rauhala E. (1992), *Nucl. Instrum. Methods* **B64**, 734.
- Sajavaara, T., Jokinen, J., Arstila, K., and Keinonen, J. (1998), *Nucl. Instrum. Methods* **B139**, 225.
- Schiettekatte, F. (2008), *Nucl. Instrum. Methods* **B266**, 1880.
- Smulders, P.J.M., and Boerma, D.O. (1987), *Nucl. Instrum. Methods* **B29**, 471.
- Spaeth, C., Richter, F., Grigull, S., and Kreissig, U. (1998), *Nucl. Instrum. Methods* **B140**, 243.
- Szilágyi, E., Pászti, F., and Amsel, G. (1995), *Nucl. Instrum. Methods*. **B100**, 103.
- Szilágyi, E. (2000), *Nucl. Instrum. Methods* **B161–163**, 37.
- Tesmer, J.R., and Nastasi, M. (eds.) (1995), *Handbook of Modern Ion Beam Materials Analysis*, Materials Research Society, Pittsburgh, PA.
- Tosaki, M., Ito, S., and Maeda, N. (2000), *Nucl. Instrum. Methods* **B168**, 543.
- Tschalär, C. (1968a), *Nucl. Instrum. Methods* **61**, 141.
- Tschalär, C. (1968b), *Nucl. Instrum. Methods* **64**, 237.
- Tschalär, C., and Maccabee, H.D. (1970), *Phys. Rev.* **B1**, 2863.
- Van Espen, P., Nullens, H., and Adams, F. (1977), *Nucl. Instrum. Methods* **145**, 579.
- Vickridge, I., and Amsel, G. (1990), *Nucl. Instrum. Methods* **B45**, 6.
- Wielopolski, L., and Gardner, R.P. (1976), *Nucl. Instrum. Methods* **133**, 303.
- Wielopolski, L., and Gardner, R.P. (1977), *Nucl. Instrum. Methods* **140**, 297.
- Yang, Q., O'Connor, D.J., and Wang, Z. (1991), *Nucl. Instrum. Methods* **B61**, 149.
- Ziegler, J.F., Lever, R.F., and Hirvonen, J.K. (1976), “Computer Analysis of Nuclear Backscattering”, in *Ion Beam Surface Layer Analysis* (Meyer, O., Linker, G., and Käppeler, F., eds.), Plenum, New York, vol. 1, p. 163.
- Ziegler, J.F. (2004), *Nucl. Instrum. Methods* **B219–220**, 1027.
- Ziegler, J.F., Biersack, J.P., and Ziegler, M.D. (2008), *SRIM: The Stopping and Range of Ions in Matter*, Lulu Press, Morrisville, NC.